NRL Report 7269

Some Possible Propagation-Associated Constraints on ELF Communications

JOHN R. DAVIS, EDWIN L. ALTHOUSE, AND DONALD R. UFFELMAN

Electromagnetic Propagation Branch
Communications Sciences Division

July 14, 1971

NAVAL RESEARCH LABORATORY
Washington, D.C.

Security Classification

DOCUMENT CONTROL DATA - R & D

(Security classification of title, body of abstract and indexing annotation must be entered when the overall report is classified)

1. ORIGINATING ACTIVITY (Corporate author)	2a. REPORT SECURITY CLASSIFICATION
Naval Research Laboratory Washington, D.C. 20390	Unclassified
	2b. GROUP

3. REPORT TITLE

SOME POSSIBLE PROPAGATION-ASSOCIATED CONSTRAINTS ON ELF COMMUNICATIONS

4. DESCRIPTIVE NOTES (Type of report and inclusive dates)

A final report on one phase of the problem; work on other phases continues.

5. AUTHOR(S) (First name, middle initial, last name)

John R. Davis, Edwin L. Althouse, and Donald R. Uffelman

6. REPORT DATE	7a. TOTAL NO. OF PAGES	7b. NO. OF REFS
July 14, 1971	40	33

8a. CONTRACT OR GRANT NO.	9a. ORIGINATOR'S REPORT NUMBER(S)
NRL Problem R07-23	
b. PROJECT NO.	NRL Report 7269
RF 14-222-401-4355	
c.	9b. OTHER REPORT NO(S) (Any other numbers that may be assigned this report)
d.	

10. DISTRIBUTION STATEMENT

Approved for public release; distribution unlimited.

11. SUPPLEMENTARY NOTES	12. SPONSORING MILITARY ACTIVITY
	Department of the Navy Office of Naval Research Arlington, Virginia 22217

13. ABSTRACT

The first phase of a study directed toward determining the effects of the propagation medium on a possible ELF communications system has been completed. A review of current theory and of the small amount of appropriate experimental information available shows that a large degree of uncertainty must be resolved before it can be considered that the characteristics of ELF propagation, even under simple, idealized ionospheric conditions, are understood.

Likely extremes of propagation-associated uncertainties in ELF communications reliability and the probable occurrence of bidirectional propagation were considered.

Theoretical calculations based on realistic ionospheric charged-particle-density models were used to acquire estimates of the likely extremes of anomalously high attenuation and strong dispersion which may occur due to standing waves between the D layer and higher ionospheric layers, particularly at night. Auroral sporadic E layers, solar flares, polar-cap absorption events, and high-altitude nuclear explosions are possible sources of such effects.

Assuming that these phenomena can indeed give rise to narrow-band resonances at certain frequencies in the ELF band, one can illustrate by sample calculations the severity of signal dispersion effects which may result. Estimates were made of the spectral contamination and dispersion which may be imposed on ELF signals both in crossing a wavy ocean surface and in penetrating depths of hundreds of meters.

DD FORM 1 NOV 65 1473 (PAGE 1)

S/N 0101-807-6801

Security Classification

14. KEY WORDS	LINK A		LINK B		LINK C	
	ROLE	WT	ROLE	WT	ROLE	WT
Communications						
ELF						
Propagation-associated constraints						
Ionospheric D and E layers						
Sporadic E layer						
Ionospheric disturbances						
Spectral dispersion and contamination						
Ocean-surface penetration						
Charged-particle-density profiles						
Attenuation rate						
Schumann resonances						
CW transmissions						
Bidirectional propagation						
Multilayer resonance effects						
Ionospheric discontinuities						
Trans-surface propagation						
Geomagnetic nonreciprocity						
Day/night asymmetry						
Earth-ionosphere waveguide						
Water-wave spectral contamination						
Geomagnetic anisotropy						
Diurnal anisotropy						
Pulse distortion						

CONTENTS

ABSTRACT

The first phase of a study directed toward determining the effects of the propagation medium on a possible ELF communications system has been completed. A review of current theory and of the small amount of appropriate experimental information available shows that a large degree of uncertainty must be resolved before it can be considered that the characteristics of ELF propagation, even under simple, idealized ionospheric conditions, are understood.

Likely extremes of propagation-associated uncertainties in ELF communications reliability and the probable occurrence of bidirectional propagation were considered.

Theoretical calculations based on realistic ionospheric charged-particle-density models were used to acquire estimates of the likely extremes of anomalously high attenuation and strong dispersion which may occur due to standing waves between the D layer and higher ionospheric layers, particularly at night. Auroral sporadic E layers, solar flares, polar-cap absorption events, and high-altitude nuclear explosions are possible sources of such effects.

Assuming that these phenomena can indeed give rise to narrow-band resonances at certain frequencies in the ELF band, one can illustrate by sample calculations the severity of signal dispersion effects which may result. Estimates were made of the spectral contamination and dispersion which may be imposed on ELF signals both in crossing a wavy ocean surface and in penetrating depths of hundreds of meters.

PROBLEM STATUS

This is a final report on one phase of the problem; work on other phases continues.

AUTHORIZATION

NRL Problem R07-23
ONR Project RF 14-222-401-4355

Manuscript submitted February 24, 1971.

SOME POSSIBLE PROPAGATION-ASSOCIATED CONSTRAINTS ON ELF COMMUNICATIONS

INTRODUCTION

Background

Under currently accepted understanding of the mechanisms available for global information transmission, extremely-low-frequency (ELF) electromagnetic waves seem attractive for communication between surface or airborne terminals and submerged submarines traveling at operational depth and speed. The Naval Research Laboratory accordingly has undertaken an investigation of the media through which ELF waves are transmitted, notably the earth's upper atmosphere and ocean surface layer, in an effort to discern and assess the likely limitations imposed by these media on information transmission. This report describes the results of a preliminary phase of this investigation in which recent developments in ELF propagation theory, together with known aspects of ionospheric physics and the physics of electromagnetic-wave transmission across sharply bounded interfaces, have been applied to the general problem of ELF communications.

In the second subsection of this introduction a brief survey is presented of experimental measurements which have been directed at determining propagation constants appropriate to ELF propagation in the earth-ionosphere waveguide. Inasmuch as these results rely heavily on natural phenomena and cannot always be related directly to a point-to-point communication situation, some comments are included to indicate their shortcomings.

The third subsection of this introduction contains a survey of attempts by several workers to calculate the appropriate propagation parameters from a theoretical basis. The diversity of approaches which have been adapted has led to an equally broad diversity of calculated results, and these results are listed to indicate the rather large uncertainty which must be resolved before it can be claimed that the characteristics of ELF propagation, even under simple, idealized ionospheric conditions, are understood.

The final subsection of this introduction contains a description of the specific problem areas, principally involving ionospheric effects on propagation, which must be investigated both theoretically and experimentally before ELF propagation under ionospheric conditions even remotely approaching realistic ones can be claimed to be understood. These problem areas form the basis for NRL's current ELF-propagation research program. They are discussed from a physical standpoint in the second section of this report, and their implications regarding the transmission of information are treated in the third section.

A Survey of Experimental Measurements of ELF Propagation Parameters

As is common in discussing earth-ionosphere waveguide propagation, the modulus of the propagation constant or wave number k will be written as a product of a (scalar) free-space wave number k_0 and a complex factor S. Propagation will be assumed to be

in the direction $\hat{\rho}$, such that $\mathbf{k} \cdot \mathbf{r} = k_0 S \hat{\rho} \cdot \mathbf{r}$, where $\hat{\rho}$ is a unit vector. The real part of S is the phase factor and is equal to the ratio of the speed of light in vacuo (c) to the electromagnetic-wave phase velocity (v_Φ). The imaginary part of S is the attenuation factor and will be given in units of dB per 1000 km.

Measurements of ELF propagation constants have relied on three sources: discrete atmospherics, Schumann resonances, and artificial continuous-wave (CW) transmissions. Of these sources, investigations of discrete atmospherics have been the most intense, whereas studies of CW transmissions have been extremely sketchy. The prominent results of each of these three types of measurements are listed below.

1. Measurements of Atmospherics

Measurement of atmospherics relies on assessment of the ELF components of a lightning pulse after transit of a path length of several thousand kilometers. Because the ELF components suffer greater delay than the higher frequency (VLF) components of atmospherics, they arrive later than the latter and constitute what is known as the "slow tail." Most such waveforms are around 20 msec long; hence these measurements provide information only at frequencies above 50 Hz or so. They are responsible for a good deal of controversy involving interpretation and are subject to rather high probable error.

Chapman and Macario (1) acquired the first quantitative results which purported to set values for ELF attenuation constants. The data were acquired from amplitude spectra of waveforms originating up to 4000 km from the receiver, although most data seem to have come from a distance less than 3000 km. Values for the attenuation constant were presented for frequencies above 100 Hz. The estimated value at 100 Hz was about 0.7 dB/1000 km and appeared to be somewhat higher in daytime than at night.

Chapman et al. (2) presented refined and extended values of propagation constants using a similar method. Once again, atmospherics yielded quantitative data only for frequencies above 100 Hz. Values at lower frequencies were determined by interpolation between the lowest-frequency point determined from atmospherics and the highest-frequency value (33 Hz) estimated from Schumann resonances. Thus they suffer the added uncertainty of being strongly dependent on the worldwide-averaged (and hence suspect) values determined from Schumann resonances. All data were acquired on north-south paths, and about 240 atmospherics were acquired. Data were confined to sources within about 2500 km. The estimated attenuation constant at 50 Hz is about 0.7 dB/1000 km.

Hughes (3) presented the results of an analysis of waveform shape, apparently without performing spectral decomposition, which purported to show that there is a substantial difference in easterly and westerly* attenuation rates on darkened paths at frequencies between 50 and 150 Hz. Assuming the slow-tail portion of an atmospheric waveform contains frequency components in this band, he determined a directional difference between the averaged attenuation rates over the 50- to 150-Hz band. The path lengths seemed to vary from a few thousand to at least 10,000 km, and some seemed to cross the twilight zone. It is not apparent whether an attempt was made to separate dark paths from mixed ones in which the twilight zone was crossed. All measurements were made at local midnight, however, so only the longest paths would experience this latter condition. Presumably they affected only a small amount of the data. Appearance of the waveforms led the author to suggest that Smith's (4) estimate of an averaged difference

*In this report "easterly" refers to waves propagating to the east, and "westerly" refers to waves propagating to the west.

of 1 dB/1000 km in attenuation for easterly (least attenuated) versus westerly propagating ELF waves between 50 and 150 Hz is valid.

In a later paper Hughes (5) reported further observations from known tropical storms at 6500 km west and 3300 km east of the observing site. A total of 100 spectra, corresponding to dark-path conditions in both directions (50 spectra from each storm), gave rise to consistent directional behavior. Spectra acquired on sunlit paths showed no directional characteristics. Data were analyzed by inspection of amplitude spectra with frequencies from 30 Hz to 1 kHz. Quantitative data were given only for frequencies above 100 Hz; at 100 Hz it was found that the attenuation rate for westerly propagating signals exceeds that for easterly propagating signals by about 0.5 dB/1000 km.

In other work Hughes and Thiesen (6) reported further measurements of atmospherics, with concentration on frequency components between 50 and 300 Hz, in an attempt to determine attenuation rate differences between dark and sunlit paths. Paths from South America to Hawaii (westerly) and South America to Arizona (northwesterly) were exploited, with ten pairs each of simultaneously received atmospherics under darkened and sunlit path conditions analyzed. All data were taken in 2-minute periods immediately following system calibration. Source distances were 4800 to 5900 km (northwesterly) and 8400 to 9600 km (westerly). The estimated diurnal difference in attenuation rate, averaged over the two paths at 50 Hz, was 1.5 ± 0.08 dB/1000 km, with the attenuation higher for sunlit paths than for dark paths.

Both of these paths crossed the equator. Smith (4) also has reported the results of ELF attenuation-rate measurements on transequatorial paths and has found a large diurnal difference as well. Smith's results indicate that the diurnal difference in attenuation rate is about 0.7 dB/1000 km, with the attenuation higher for sunlit paths. Because these results suggest a larger diurnal difference in attenuation rate than either theoretical predictions or other measurements, and in view of the fact that they both correspond to transequatorial paths, it is possible that they evince an anomalous propagation effect associated with the equatorial ionosphere. Further results of both these investigators, to be discussed below, tend to reinforce this hypothesis.

Hughes and Thiesen (7) in another report described an attempt to determine the effect of a discontinuity in waveguide boundary height along an ELF propagation path. The most interesting and controversial result of this work, however, arose from a series of measurements involving completely dark and completely sunlit paths. The instrumentation and receiving sites were the same as described in Ref. 6. By measuring total attenuation along each of the two separate paths and dividing by path difference, values of what they term an apparent attenuation rate (this parameter should not be interpreted as a true attenuation rate) of 3.9 dB/1000 km for 50-Hz propagation along a sunlit path and of 1.6 dB/1000 km along a dark path resulted. Twenty pairs of atmospherics were analyzed for each path condition, and the estimates were based on spectral analysis. It is noted that 50 Hz corresponds to the lower limit of spectral resolution and that the source region was in the equatorial zone. If the northwesterly path was assumed to experience an actual attenuation rate of 0.8 dB/1000 km for daytime propagation, consistent with other results quoted above, then the apparent attenuation rate of 3.9 dB/1000 km indicates that the actual value for westerly propagation on a sunlit path is slightly less than 2 dB/1000 km. Similarly, for dark path conditions, there results an estimated value for westerly propagation of slightly more than 1.1 dB/1000 km. These values, once again, are much larger than both the predictions of theory and other measurements. On similar transequatorial paths Smith (4) has found attenuation rates of 2.3 dB/1000 km and 1.6 dB/1000 km for sunlit and dark paths respectively. The trend of these values is in general agreement with those of Hughes and Thiesen (7) and reinforces the hypothesis that there occurs within the equatorial zone a propagation phenomenon which is unique to that region. The unusual magneto-ionic conditions which prevail in the equatorial lower E

layer due to the extremely high currents associated with the equatorial electrojet may contain the explanation of this phenomenon.

Jones (8) considered the spectral dispersion of impulsive electromagnetic pulses in the earth-ionosphere waveguide and obtained temporal-domain waveforms for the expected resultant atmospherics traveling via both long and short great-circle paths from a postulated source to a given receiver position. Noting that the rather complex wave shapes which the superposition of these two components should yield are not in fact observed experimentally, he suggested that the attenuation rate may well be larger than that which is expected (namely 0.6 to 0.8 dB/1000 km).

Taylor and Sao (9) reported measurements of 40 pairs of waveforms acquired simultaneously on easterly (Pacific Ocean to Colorado) and westerly (Pacific Ocean to Japan) paths under dark-path conditions. Amplitude spectra were acquired and attenuation rates estimated for frequencies between 20 and 400 Hz. Data below 50 Hz probably are invalid. The difference in attenuation rates was a minimum at 50 Hz, where the easterly value was estimated to be 0.75 dB/1000 km and the westerly value was estimated to be 0.93 dB/1000 km. The authors took note of the highly inaccurate methods and small sample of data and suggested that the rather large probable error (the margin of error encompasses both values at every frequency) casts a great deal of doubt on the results.

In summary, studies of atmospherics have not yielded altogether consistent results for ELF attenuation rates. References 1 and 2 contain results for relatively short, temperate-zone north-south paths which indicate a value of 0.7 dB/1000 km in the 50- to 100-Hz region. References 3 through 9 indicate that there are propagation asymmetries for easterly and westerly propagation as well as for darkened and sunlit paths. These references also indicate that attenuation rates in the 50- to 100-Hz band may be as great as 1.5 to 2.0 dB/1000 km, although the interposition of the equatorial zone in the paths used for many of these measurements casts some doubt on their validity.* Beneath all the results derived from measurements of atmospherics, of course, there runs a substantial undercurrent of suspicion. The 50- to 100-Hz region is at the low-frequency extreme of the band which can be investigated by use of atmospherics. Indeed, some of the results quoted above were determined by interpolation between the lowest-frequency values estimated by observations of atmospherics and the highest-frequency values estimated from observations of Schumann resonances. The latter is a phenomenon of global scale, as is mentioned below, and hence casts further suspicion on the validity of these figures.

2. Measurements of Schumann Resonances

Measurements of Schumann resonances rely on theoretical calculation of the effective conductivity of an assumed model ionospheric boundary to the earth-ionospheric waveguide, based on measurements of the frequencies of Schumann resonances. Several difficulties are associated with this method, and the results are highly uncertain. Because the Schumann resonances are a worldwide phenomenon, any results determined from them must be considered gross averages over all times of day, seasons, and geomagnetic-field orientations. A suggestion that such effects probably are important may be gathered from the circumstance that the measured frequencies of Schumann resonances vary by several percent, systematically, over a period of a day. Furthermore, since the signal-to-noise ratio for the resonant-mode amplitudes declines rapidly with frequency, the most reliable results arise from the fundamental resonance mode (at about 8 Hz); data have been used for modes as high as the fifth (at about 33 Hz), however.

*It should be noted, however, that even if some anomalous propagation phenomenon in the equatorial zone is responsible for these high attenuation rates, this phenomenon remains a matter of vital concern for a global communications system and cannot simply be disregarded.

Chapman and Jones (10) presented the theoretical basis for interpreting Schumann resonances in terms of a simple, two-layer ionospheric model to yield the effective boundary conductivity which is necessary for estimating ELF attenuation rates from them. They also presented a collection of results based on other models. A one-year collection of data (about 500 spectra) yielded estimates of attenuation rates between 1 and 1000 Hz. At 50 Hz there resulted an estimate of 0.7 dB/1000 km.

3. Measurements of CW Transmissions

Due to the technical difficulties of radiating energy in the ELF band at high enough power to be detected at ranges of thousands of kilometers, very few data have been gathered for CW transmissions. In the case cited below, CW transmissions were detected on path lengths of a few thousand kilometers, and measured values of attenuation rate and phase velocity were acquired for a frequency of 400 Hz.

Dunn et al. (11) and Kuhnle and Smith (12) used a rented 67-mile section of power transmission line on the California-Nevada border (oriented roughly in an east-west direction), grounded at both ends, to radiate a 400-Hz continuous wave at 300-kw input power. Measurements on an easterly path were made in Utah (500-km range), Michigan (3000-km range), and New York (4000-km range). Both nighttime and daytime path conditions, as well as the sunrise transition period, were investigated. Signal levels at 400 Hz were high enough at the receiver sites that coherent integration times of 1 to 4 seconds gave satisfactory results. The measured attenuation constants of 3 to 3.5 dB/1000 km for nighttime propagation and 7.8 to 9.0 dB/1000 km for daytime propagation are both somewhat larger than predicted by theory. There was evidence that during the night-day transition period a smooth transition from the usual nighttime received signal level to the daytime value did not occur but that the signal experienced rather deep fading (as deep as 20 dB) for a while, followed by recovery to the usual daytime level. This behavior indicates that the ionospheric twilight zone probably does cause a modal interference effect in ELF wave fields below the transition region.

A Survey of Theoretical Calculations of ELF Propagation Parameters

Calculations of ELF attenuation rates have undergone a substantial process of refinement since the simple, two-layer model of Chapman and Jones (10) was constructed as an attempt to force-fit a crude ionospheric conductivity profile to their Schumann resonance data cited previously. Although this two-layer model succeeded in fitting both the positions of the Schumann resonances in the frequency domain and their effective Q-factors, it was not claimed as a realistic representation of the true lower ionosphere. Subsequent efforts by Galejs (13-17), Field (18), Yamashita (19-20), and Jones (21) have progressively included greater complexity and realism and have provided estimates of ELF attenuation constants which display day/night and east/west propagation asymmetry and which cover a wide range of values. Table 1 contains a digest of the values obtained in these studies for the particular frequencies of 45 and 75 Hz, two frequencies of possible interest for experiment on which the applications described in this report have been concentrated. To permit a comparison to be made between the diversity of approaches taken by these workers, the entries have been arranged according to their similarity in geometric configuration and are annotated briefly to indicate this configuration as well as other pertinent characteristics such as the magnetic-field treatment and the inclusion or exclusion of ions. The values for attenuation rate are quoted in dB per 1000 km with the following shorthand notation:

Table 1
Some Calculated Values of ELF Attenuation Constants (dB/1000 km)

Source and Comments	Frequency = 45 Hz						Frequency = 75 Hz					
	α_{EW}		α_{WE}		α_{ISO}	α_{FLD}	α_{EW}		α_{WE}		α_{ISO}	α_{FLD}
	Day	Night	Day	Night			Day	Night	Day	Night		
Galejs (13) flat earth, horizontal field, no ions	0.66	0.59	0.52	0.42	NS Day 0.59	NS Night 0.52	0.64	0.60	0.53	0.42	NS Day 0.61	NS Night 0.52
Jones (21) flat earth, no field:												
(a) Cole/Pierce (22) profile; no ions	—	—	—	—	0.60	—	—	—	—	—	1.00	—
(b) Cole/Pierce (22) profile; ions included	—	—	—	—	0.40	—	—	—	—	—	0.70	—
(c) Deeks (23) profile	—	—	—	—	0.80	—	—	—	—	—	1.10	—
(d) Deeks (23) profile; ions from (22)	—	—	—	—	0.70	—	—	—	—	—	1.00	—
(e) Artificial two-layer profile	—	—	—	—	0.70	—	—	—	—	—	1.00	—
Field (18) flat earth, horizontal field: no ions	0.50	—	—	—	—	—	0.90	—	—	—	—	—
$N_i \leq 5\times10^3$ cm^{-3}	0.80	1.10	0.80	1.10	—	—	1.10	1.40	1.10	1.30	—	—
$N_i \leq 8\times10^3$ cm^{-3}	0.90	—	—	—	—	—	1.20	—	—	—	—	—
$N_i \leq 2\times10^4$ cm^{-3}	1.10	—	—	—	—	—	1.60	—	—	—	—	—
Galejs (15) cylindrical earth; dipping field, no ions (Deeks (23) profile)	0.60	0.80	0.60	(Note: resolution is poor on these illustrations) 0.80	—	—	1.30	1.10	1.10	1.10	—	—
Galejs (17) cylindrical earth, no field; ions of following densities:	(Disregard column labels above for these entries under Ref. 17)											
	e	e + i MW = 29	e + i MW = 60	e + i MW = 60			e	e + i MW = 29	e + i MW = 60	e + i MW = 60		
$N_i \leq 10^3$ cm^{-3}	0.50	0.70	0.60	0.56			0.85	1.05	1.00	0.90		
$N_i \leq 10^4$ cm^{-3}		1.10		0.66				1.80		1.00		
$N_i \leq 10^5$ cm^{-3}		1.80		1.10				2.40		1.40		
$N_i \leq 10^6$ cm^{-3}		1.70		1.70				2.40		2.40		
Yamashita (19) spherical earth, radial field, no ions, single layer	—	—	—	—	0.45	0.90	—	—	—	—	0.60	1.10
Yamashita (20) spherical earth, radial field, no ions, two layers	—	—	—	—	—	1.70	—	—	—	—	—	2.40
Galejs (14) spherical earth, radial field, no ions	(Disregard column labels above for these entries under Ref. 14)											
	Day ISO	Night ISO	Day FLD	Night FLD			Day ISO	Night ISO	Day FLD	Night FLD		
	0.58	0.41	0.75	0.70			0.90	0.70	1.05	1.00		

α_{EW} corresponds to westerly propagation;

α_{WE} corresponds to easterly propagation;

α_{ISO} corresponds to propagation in the absence of a geomagnetic field;

α_{FLD} corresponds to propagation in the presence of a geomagnetic field in which there is no geomagnetic anisotropy.

Values for both darkened and sunlit paths are given where available. In several cases in which the calculations do not fit the format of the table, additional notations are included in the individual data blocks. A brief explanation of each treatment listed in Table 1 is given below.

The values abstracted from Ref. 13 were calculated on the basis of a flat earth and horizontal north-south geomagnetic field, neglecting the effects of ions. The ionospheric model was constructed from typical electron-density and collision-frequency profiles. Values in the columns of Table 1 correspond to the column headings except for the last two entries for each frequency. These entries correspond to north-south (and hence isotropic or field-free) propagation on sunlit and darkened paths respectively. The values abstracted from Ref. 21, also for a flat-earth case, are all for isotropic conditions in which the geomagnetic field is neglected. The four entries at each frequency, from Cole and Pierce (22) and Deeks (23), are intended to cover typical realistic ionospheres with and without the inclusion of ions. The fifth entry corresponds to the artificial two-layer model of Chapman and Jones (10). The values abstracted from Ref. 18, also for a flat earth and with a similar horizontal geomagnetic field to that employed by Galejs (13), are intended to illustrate the effects of increasing ion density, which might be encountered at higher latitudes. The designation N_i in each entry indicates the approximate maximum negative-ion density achieved at about a 30- to 40-km altitude. The cases of no ions and $N_i \lesssim 5\times10^3$ cm^{-3} correspond to low latitudes.

The cylindrical-earth examples abstracted from Refs. 15 and 17 also are intended to illustrate the importance of low-altitude ions. The entries in the former case are self-explanatory, but in the latter case they correspond to completely different categories than indicated by the column headings. For this reason, labels are inserted above these entries. Those in the column labeled "e" are based on no ions at all; those in the column labeled "e + i, MW = 29" are based on electrons plus ions of atomic mass 29; those in the first column labeled "e + i, MW = 60" are based on electrons plus ions of atomic mass 60 (such as might be encountered in an aerosol or a concentration of water cluster ions); those in the second column labeled "e + i, MW = 60" are based on the same charged-particle distribution as the preceding column but with an ion-neutral collision frequency of twice the neutral-neutral collision frequency.

The spherical-earth examples abstracted from Refs. 19 and 20, with no ions and an assumed radial geomagnetic field, correspond to one- and two-layer ionospheric models, respectively, of a similar type to those employed by Chapman and Jones (10). Although these entries are suspect because they are based on unrealistic, sharply bounded ionospheric layers, they are of interest because they depart significantly from those determined by Chapman and Jones (10). These models enjoy reasonable success in explaining observed characteristics of slow-tail atmospherics, nevertheless, and hence point out that even this oversimplified method of describing the earth-ionosphere waveguide is capable of producing a large discrepancy in calculated attenuation coefficients.

The spherical-earth examples abstracted from Ref. 14, also corresponding to a radial geomagnetic field and no ions, were based on a more realistic ionospheric model (the same one as was used in Ref. 13). Once again, because the geomagnetic field was

approximated by its radial component, there is no distinction between easterly and westerly propagation. The entries do not properly fit the format of the table consequently, and labels have been inserted above the entries to indicate their actual significance. The labels are self-explanatory and are consistent with terminology previously explained.

The diversity of results among the approaches represented in Table 1 demonstrates emphatically the chaotic state of theoretical ELF attenuation-rate calculations. Two cases in point illustrate this circumstance:

- References 13 and 14, in which propagation on sunlit and darkened paths can be compared, show that attenuation rates for the former generally exceed those for the latter by an average of about 20% at 45 Hz, whereas Refs. 15 and 18 show that those for the latter generally exceed those for the former by 35%.

- References 17 and 18 indicate that inclusion of ions generally results in an increase of attenuation coefficient, whereas Ref. 21 suggests the contrary.

There are two significant areas of consistency among the results as well:

- Inclusion of the geomagnetic field generally leads to increased estimates of attenuation rate at 45 Hz by 30 to 100% over the isotropic case.

- Attenuation rates for westerly propagation exceed those for easterly propagation at 45 Hz by an average of 30% at temperate latitudes.

Values of attenuation coefficients for all conditions vary from 0.4 to 1.8 dB/1000 km at 45 Hz, and from 0.6 to 2.4 dB/1000 km at 75 Hz. The absence of systematic trends in their dependence either on the presence or absence of ions or on the condition of path illumination makes it impossible to assess the effects of geographic path location. The slight trend of evidence concerning the effect of the geomagnetic field suggests that propagation may indeed be expected to be anisotropic with a difference in attenuation rate of as much as 30%.

Problem Areas of Interest for Research

The possible irregularities and anisotropies of propagation whose existence is suggested by the examples discussed in the prior two parts of this introduction must be investigated experimentally if their effects on ELF propagation are to be fully understood. The object of the research reported here is to apply current theoretical suppositions to circumstances likely to be encountered in global communications and thereby to discern the probable limits of degradation that these propagation-related phenomena will have on information transmission.

Table 2 lists four prominent categories into which such degrading phenomena may be grouped and nine subcategories, either of specific physical mechanisms or of the consequences of such mechanisms, which may be conveniently isolated for theoretical study.

The two items listed under Bidirectional Propagation are of importance because the low attenuation constants expected at ELF should permit energy from both the direct (short great circle) and antipodal (long great circle) paths to propagate to much of the world. The spatial interference pattern which results may cause wave-field fluctuations of 3 to 6 dB thousands of kilometers in scale at ranges beyond about 10,000 km. This matter is discussed more thoroughly by Kelly (24), and only a few representative examples of the possible extremes will be listed in the following section.

Table 2
Problem Areas for ELF Propagation Research

Bidirectional Propagation
• Geomagnetic nonreciprocity
• Day-night asymmetry
Multilayer Resonance Effects
• Anomalous high attenuation
• Dispersion
Ionospheric Discontinuities
• Height changes at twilight zone
• Interposed conducting layers such as sporadic E
• Solar and nuclear perturbations
Trans-Surface and Subsurface Propagation
• Water-wave spectral contamination
• Dispersion

Multilayer Resonance Effects arise because the extremely long wavelengths characteristic of ELF waves can cause energy to penetrate tens to hundreds of kilometers above the D and lower E regions where reflection is commonly considered to occur. The existence of higher layers then can cause standing waves to be set up which may create resonance-associated absorption maxima in certain frequency bands a few hertz wide. The existence of these attenuation peaks may introduce substantial dispersion into a signal which occupies the same portion of the spectrum. This matter was first described by Galejs (25), and the bulk of the material in the following two sections represents application of the theory to ionospheric configurations which may be encountered in a communications environment.

The items listed under Ionospheric Discontinuities involve primarily local wavefield irregularities which may occur due to mode conversion within a few hundred to a thousand kilometers of the three sources of ionospheric-boundary height changes indicated. Height changes of about 20 km will be encountered at the twilight zone, for example, and may create a modal interference pattern in this transition region which will greatly complicate communications to receivers located within it. The limited experience with 400-Hz CW transmission that was mentioned in the second subsection of this introduction confirms that passage of the twilight zone across an ELF transmission path can cause the deep fading which is characteristic of such an effect. Interposed conducting layers of hundreds to thousands of kilometers extent, such as sporadic E layers, can be expected to cause equally degrading effects when they occur on an ELF transmission path at night. During nighttime, ELF wave fields penetrate well above the D layer and hence may be highly susceptible to such occurrences. This possibility is of substantial concern because both the equatorial and auroral zones are regularly subject to the occurrence of sporadic E layers. Some of the material regarding measurements of atmospherics that were presented in the second subsection suggests that such anomalous propagation effects may occur in the equatorial zone (4,7).

Solar flares, polar-cap absorption (PCA) events, and high-altitude nuclear explosions can be expected to cause similar effects. None of these three phenomena will be discussed as types of ionospheric discontinuities in the following two sections. They are subjects of investigation in NRL's ELF research program, however, and are being pursued currently.

The two listings under Trans-Surface and Subsurface Propagation relate to the effects of the ocean on ELF waves traversing its boundary and penetrating to a submerged receiver hundreds of meters deep. Spectral contamination can be expected to arise from the modulation effect of water waves on the surface, and signal dispersion will result from the frequency-dependent character of attenuation in water. Examples of both of these effects will be given in the third section of this report.

SOME ASPECTS OF ELF PROPAGATION PHYSICS

Figure 1 illustrates schematically the extent to which several of the possible propagation-associated phenomena described in the introduction may affect ELF wave fields on a global scale. The ionosphere in the darkened hemisphere (on the right) is higher, effectively, than that in the sunlit hemisphere (of course, all heights are grossly distorted for ease of illustration). The stippled region, which appears between the ionospheric boundary and the surface of the earth (the circle in the center), represents an estimate of wave-field magnitude on the earth's surface at 45 Hz. The heavy line which bounds this region indicates, on an approximate 30-dB scale, the extent to which bidirectional propagation effects are expected to be of importance. Nulls as much as 20 dB deep, separated by 2500 to 3000 km, are prevalent at ranges beyond 10,000 km. Near the transmitter and extending out to 1000 km or so on either side, the near field dominates. Areas of similar size occur in the twilight zone and at the antipode, in which modal interference effects may be expected to cause a substantial degree of spatial and temporal irregularity in the wave fields. In addition to these more-or-less regular and continuous effects, ionospheric irregularities, sporadic E layers at both the polar and equatorial regions, and other solar/geomagnetic phenomena can be expected to create additional irregular structure thousands of kilometers in scale. The thrust of Fig. 1 is simply to illustrate, schematically, that much of the world may be expected to be subject to the influence of the phenomena discussed in this report.

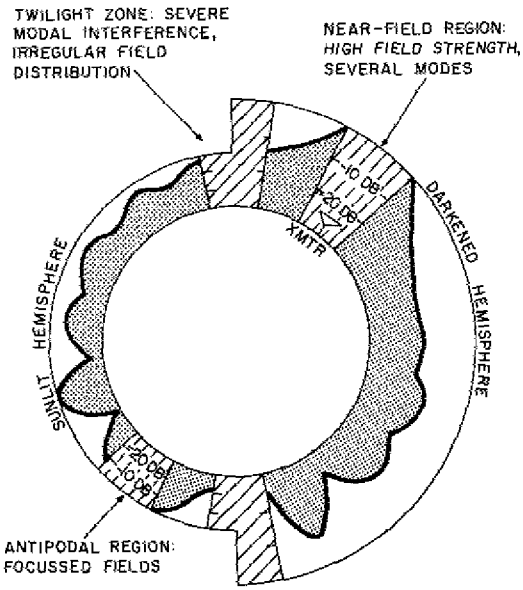

Fig. 1 - Schematic representation of the propagation-associated wave-field distribution.

Bidirectional Propagation

Bidirectional propagation is treated in detail by Kelly (24), and the intent here is only to present a few illustrative examples of the importance which may reside in bidirectional propagation effects at 45 and 75 Hz.

Figure 2 shows the far-field azimuthal component of the 45-Hz magnetic field (H_ϕ) relative to its value at 1000 km from the transmitter. The wave-field profile is extended to 19,000 km, beyond which

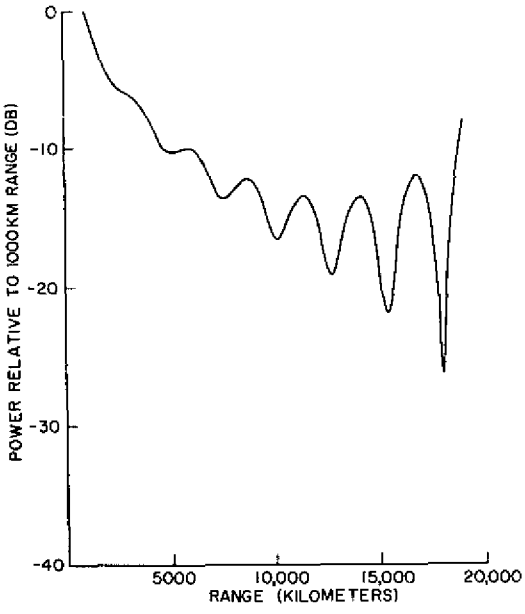

Fig. 2 - Far-field azimuthal component of the magnetic field at 45 Hz, with no geographical asymmetry

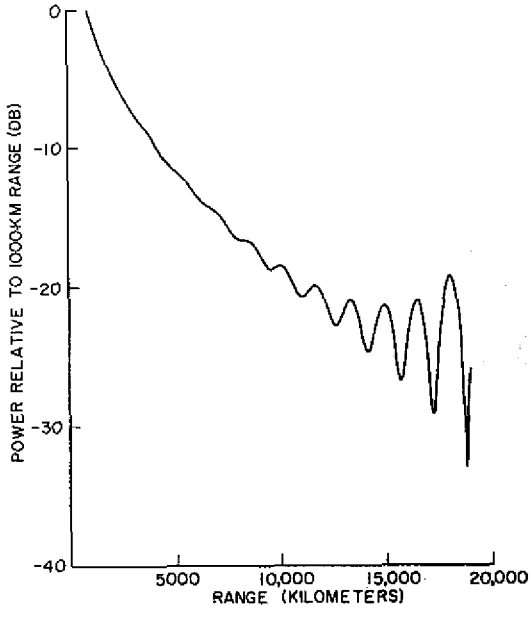

Fig. 3 - Far-field azimuthal component of the magnetic field at 75 Hz, with no geographical asymmetry

antipodal effects make the far-field expression invalid. This curve was calculated on the basis of an assumed isotropic attenuation rate of 0.7 dB/1000 km, and shows quite clearly that bidirectional propagation must be considered, under even this most simple of circumstances, at ranges of 10,000 km and beyond. Figure 3 shows a similar curve for 75 Hz, based on an assumed isotropic attenuation rate of 1.2 dB/1000 km. Once again, bidirectional propagation effects become important at ranges of 10,000 km and beyond. These two examples were based on optimistic, estimated values of attenuation rate and hence represent a conservative indication of likely effects.

Figure 4 shows the effect of introducing an additional 0.17-dB/1000-km attenuation rate into the short great-circle path, such as might very reasonably result from a geomagnetic nonreciprocity in propagation. This curve for 45 Hz indicates that bidirectional propagation effects must be considered important at ranges of 8000 km and further. Figure 5 shows similar results for 75 Hz, in which 0.56 dB/1000 km has been added to the short-path attenuation rate. (The attenuation rates and phase velocities for the calculations shown in Figs. 4 and 5 are consistent with those determined by Galejs (26).)

Figure 6 contains results of calculations for a more complicated case, in which the intent is to show possible effects both of geomagnetic nonreciprocity and day/night asymmetry. The 45-Hz transmitter is assumed to be 2000 km from the twilight zone and in the darkened hemisphere. Transmission across the twilight zone is assumed to be complete, an expedient which probably causes field strengths to be overestimated. The ranges shown on the horizontal scale are measured from the twilight zone and in the sunlit hemisphere. Attenuation in the darkened hemisphere (which is assumed here to coincide with an easterly, long great-circle path) is assumed to be 0.4 dB/1000 km. Attenuation in the sunlit hemisphere (a westerly, short great-circle path) is assumed to be 0.8 dB/1000 km. These values probably represent the reasonable extreme in geographic-path asymmetry. Notice that the interference-related nulls are much deeper in Fig. 6 than in any of the previous figures and that bidirectional propagation effects are

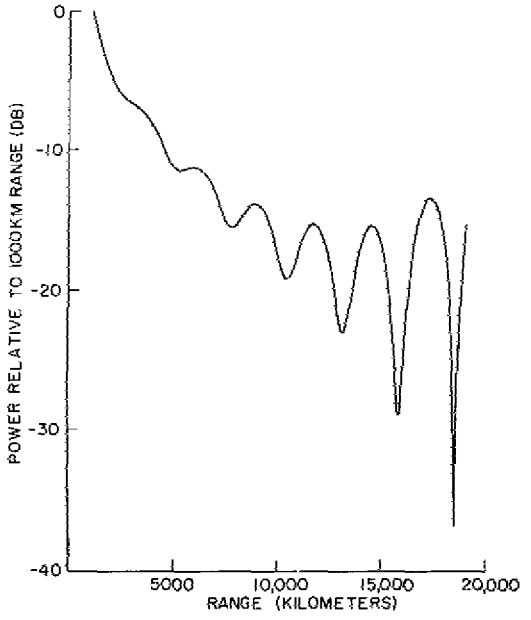

Fig. 4 - Far-field azimuthal component of the magnetic field at 45 Hz. The short-path attenuation rate is 25% higher than the long-path attenuation rate as an estimate of possible geomagnetic asymmetry.

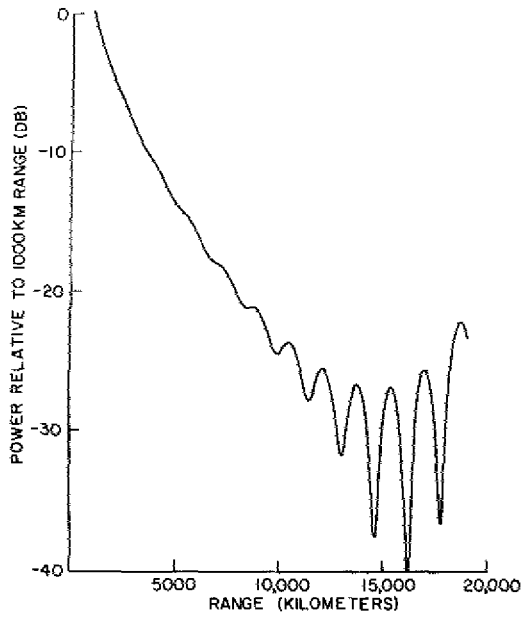

Fig. 5 - Far-field azimuthal component of the magnetic field at 75 Hz. The short-path attenuation rate is 45% higher than the long-path attenuation rate as an estimate of possible geomagnetic asymmetry.

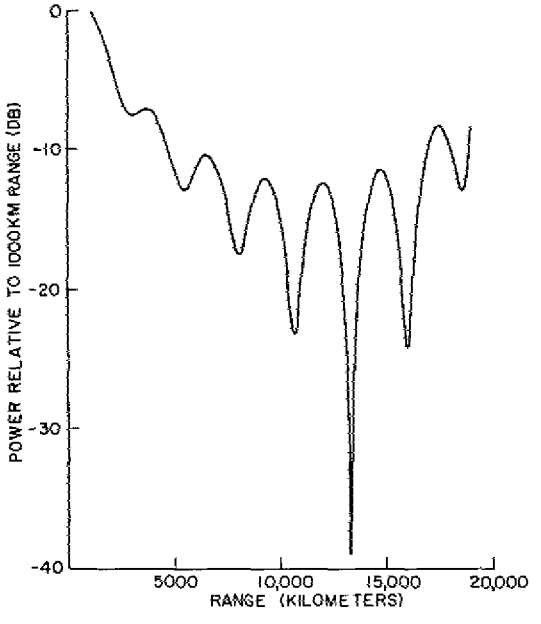

Fig. 6 - Far-field azimuthal component of the magnetic field at 45 Hz. The short-path attenuation rate is 100% higher than the long-path attenuation rate as an estimate of combined geomagnetic and day-night asymmetry.

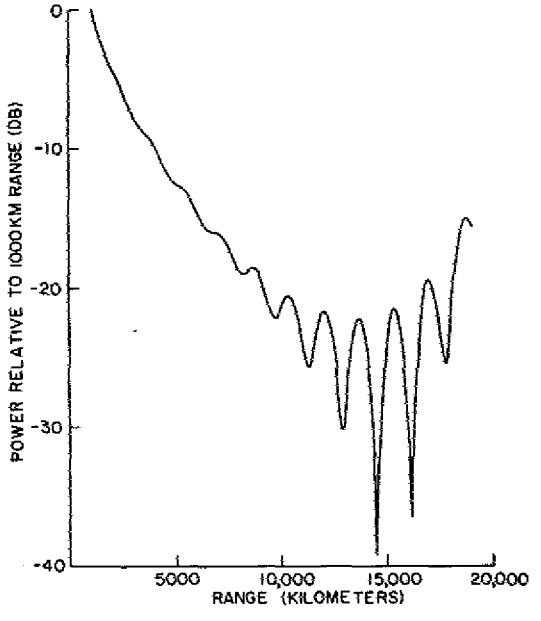

Fig. 7 - Far-field azimuthal component of the magnetic field at 75 Hz. The short-path attenuation rate is 50% higher than the long-path attenuation rate as an estimate of combined geomagnetic and day-night asymmetry.

significant nearly everywhere outside the near-field region. Figure 7 shows similar results for 75 Hz, in which attenuation on the darkened, easterly path is assumed to be 1.0 dB/1000 km and on the sunlit, westerly path is assumed to be 1.5 dB/1000 km. Once again, these figures represent a probable extreme case and indicate that bidirectional propagation effects can be important at ranges as close as 6000 km.

Multilayer Resonance Effects

As Galejs (25) has indicated, ELF propagation in the nighttime ionosphere is strongly influenced by the charged-particle distributions in the E and F layers. He has shown that, under somewhat oversimplified ionospheric conditions, standing waves are established between the D and F layers. These standing waves cause effective resonant absorption peaks to appear in frequency bands a few hertz wide, which are distributed throughout the ELF band and can fall directly on frequencies of interest for ELF communications. The oversimplification to which Galejs' calculations are subject stems primarily from the fact that the F-layer electron-density profile he has used is sharply bounded. This circumstance is a consequence of the iterative computational method Galejs has used. It is likely that more realistic F-layer electron-density models will yield less extreme, although similar, resonant effects, and a means for employing smoothly varying F-layer electron-density profiles is currently under investigation at NRL. An object of the research reported here has been to use the existing computational technique to discern likely limits of these standing-wave effects on ELF communications.

The entire region of the ionosphere above the D layer is expected to strongly influence ELF propagation under dark-path conditions. Hence the phenomena whose effects must be investigated include not only the nighttime F layer but additional nocturnal ionospheric effects such as northern-latitude sporadic E layers. Other phenomena, which are not exclusively nighttime occurrences, also must be considered. Polar-cap absorption (PCA) events, auroral absorption events, high-altitude nuclear explosions, and solar flares are examples of such phenomena. Indeed, ionospheric behavior in the auroral zone and polar cap, which includes many of the phenomena listed above, is of great likely importance for ELF communications. Figure 8 is an azimuthal equidistant projection centered in the midwestern United States and showing a possible transmitter location at the junction of the two dashed lines in northern Wisconsin. The fan-shaped area indicates paths to probable regions of operational communications interest off the coast of Asia, in the Mediterranean, in the North Sea and Baltic Sea, and in the Arctic Ocean. These areas appear in the stippled region between 3000 and 8000 naut mi (5500 to 15,000 km) from the transmitter. Also indicated on Fig. 8 are three somewhat irregularly shaped rings centered on the northern magnetic pole in the vicinity of Ellesmere Island. These rings bound the northern auroral zone and polar cap, and it is evident that all propagation paths of interest pass through this region for a distance of several thousand km. Such phenomena as nighttime sporadic E layers, which have been found to occur in the auroral region at some time during more than 50% of all periods of darkness and during more than 30% of all hours of darkness (27), thus must be investigated carefully.

As an illustration of the extent to which auroral sporadic E layers can be expected to affect ELF propagation at the frequencies of 45 and 75 Hz, Figs. 9 and 10 contain curves of apparent wavelength versus altitude for typical ionospheric electron-density profiles at these two frequencies. These curves were calculated on the basis that for waves propagating in a partially conducting medium, an apparent spatial wavelength is equal to the free-space wavelength divided by the real part of the refractive index. This criterion permits objects such as charged-particle layers in the medium to be evaluated as possible refracting or reflecting objects according to their size relative to this apparent wavelength. It is a somewhat more restrictive criterion than comparison with the skin depth, which pertains to evanescent waves.

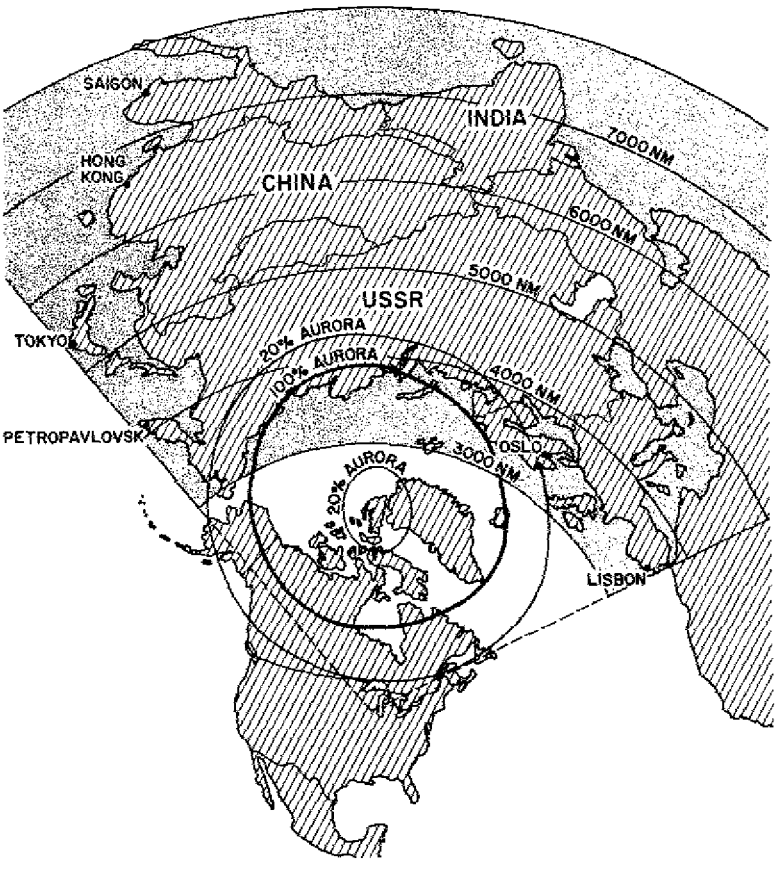

Fig. 8 – Locations of the possible communications-link propagation paths relative to the arctic auroral-zone and polar cap

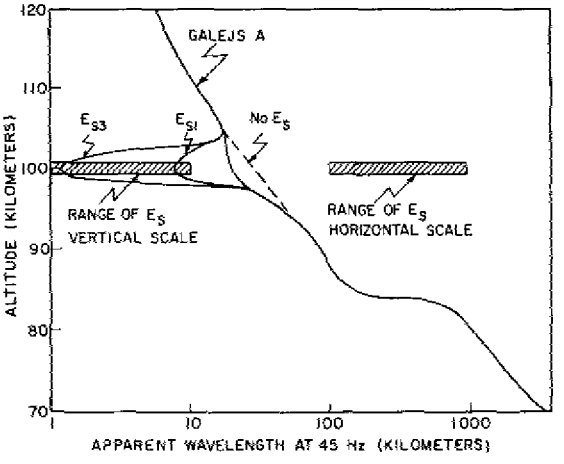

Fig. 9 – Altitude profile of the apparent electromagnetic wavelength for ELF waves of 45 Hz

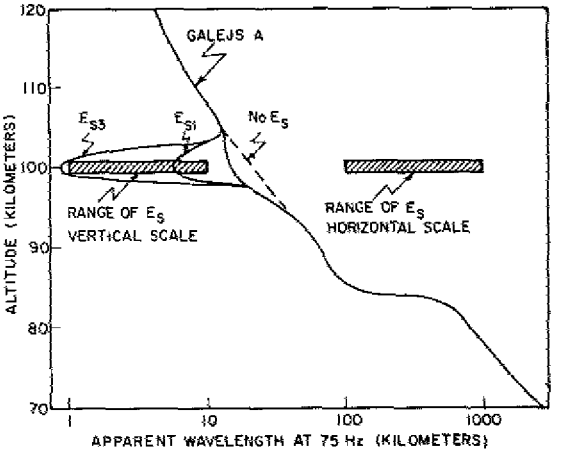

Fig. 10 – Altitude profile of the apparent electromagnetic wavelength for ELF waves of 75 Hz

The solid curve labeled "Galejs A" in each illustration is representative of typical nighttime electron-density profiles and was used for some of the calculations in Ref. 25. This curve contains a small contribution from sporadic E, and the dashed curve segment labeled "No E_S" illustrates the condition which exists in the complete absence of sporadic E layers. The two protuberances labeled E_{S1} and E_{S3} indicate the modifications to this curve which are introduced by moderate (E_{S1}) to strong (E_{S3}) nighttime sporadic E layers in the 100-km region of altitude. These modifications result in a compression of the apparent wavelengths of 45- and 75-Hz propagating waves into the 1- to 10-km scale interval. The crosshatched areas represent typical horizontal- and vertical-scale sizes for sporadic E layers at 100-km altitude. Even under a condition of moderate sporadic E layers, it is evident that such a layer displays a vertical extent comparable to an apparent wavelength at both 45 and 75 Hz. Thus even under this circumstance a sporadic E layer must be considered to be of considerable influence on ELF propagation. A strong sporadic E layer is nearly always greater in vertical extent than an ELF wavelength (especially in view of the fact that a strong layer often has a vertical extent toward the right-hand edge of the shaded region) and hence must be considered to be a nearly completely reflecting surface. It is likely that essentially no ELF energy will propagate to above the 100-km altitude region within the 100- to 1000-km horizontal dimensions of such a layer. Calculated values of ELF attenuation constants to be presented in a later section will provide further confirmation of these expectations.

The remainder of this discussion of ELF propagation physics is concerned with the influence of E- and F-layer charged-particle density configurations on attenuation constants calculated in the manner described by Galejs (25). For this reason certain of the features of Galejs' treatment should be listed. The technique is described most fully in Ref. 15. Both the electron density and collision frequency are allowed to have arbitrary height dependence in a cylindrically stratified ionosphere. The geomagnetic field is allowed to have an arbitrary angle of dip, but propagation is restricted to easterly or westerly directions. Within each stratum the differential equations for the wave fields are separable but can be solved only if the radial variable is approximated by a constant. A matrix multiplication process is used in an iterative calculation to determine the wave fields in the strata, and from these calculated wave fields the propagation factor S is computed. Errors in the computation are minimized by selecting strata to be much smaller than a radio-frequency wavelength.

For the work reported in Ref. 25, Galejs assumed a constant positive- and negative-ion density of 2000 cm^{-3} at altitudes below 64 km. Between 64 and 90 km, he used an assumed exponential height dependence of the form

$$N_- = 10^{-7.4+0.36Z-0.003Z^2} ,$$

where N_- is the negative-ion density in cm^{-3} and Z is the altitude in kilometers. Above 90 km he assumed a negative-ion density of nearly zero.

The geomagnetic field is treated as dipping at 45° at altitudes up to about 120 km; above this altitude it is treated as a radial (vertical) field. Once again this expedient is a necessary consequence of the computation method.

Figure 11 contains electron-density profiles used by Galejs (25), as well as three typical sporadic-E-layer-associated protuberances which have been investigated in the research reported here. The three sporadic E layers are superimposed on Galejs' curve A, which represents an approximation of a nighttime ionospheric electron-density profile. These electron-density profiles are the same ones which are represented in Figs. 9 and 10.

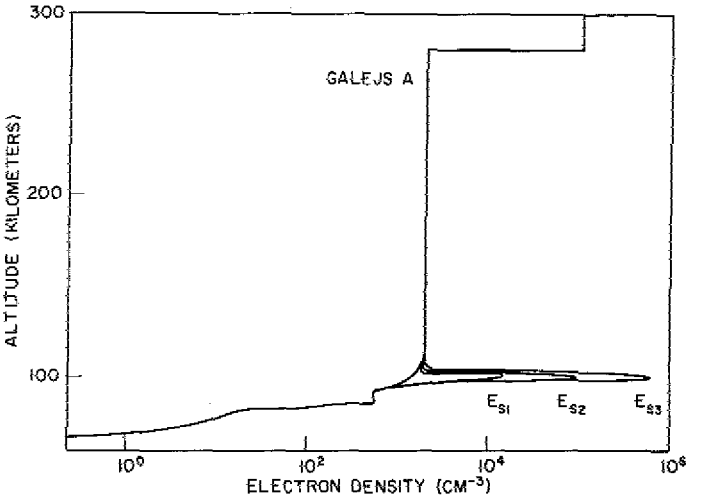

Fig. 11 – Electron-density profiles used for the propagation calculations by Galejs (25) and for various conditions of the sporadic E layer

Figure 12 contains four curves of attenuation rate α versus frequency, corresponding approximately to the four electron-density profiles illustrated in Fig. 11. (The only difference is that an F-layer height of 290 km was selected instead of the value of 280 km shown in Fig. 11.) The curve in Fig. 12 labeled "No E_S" was calculated from the "Galejs A" electron-density profile. The absence of a sporadic E layer, together with the extremely simple, almost stepped, double-layer configuration, gives rise to a strong resonance structure. Resonant attenuation peaks of 3.5 dB/1000 km at 23 Hz, 4.0 dB/1000 km at 50 Hz, and 5.6 dB/1000 km at 87 Hz indicate the pronounced standing-wave structure which results from this highly oversimplified case. As indicated by Galejs (25), the positions of these resonances in frequency can be altered substantially by slight changes of F-layer height. A shift of 20 km in this height, for example, causes a frequency shift of about 6 Hz in the resonance at 50 Hz. (Inasmuch as resonances arise at frequencies for which the interlayer separation is an integral multiple of radial half-wavelengths, layer movements yield a proportional shift in resonant wavelengths.) The strengths of the resonances are sensitive to the electron density assumed at the F-layer ledge. Increasing this electron density to 10^6, a not unreasonable value, makes the resonances many dB/1000 km stronger; decreasing it to 10^4, possibly an unreasonable lower extreme, makes them decrease by several dB/1000 km.

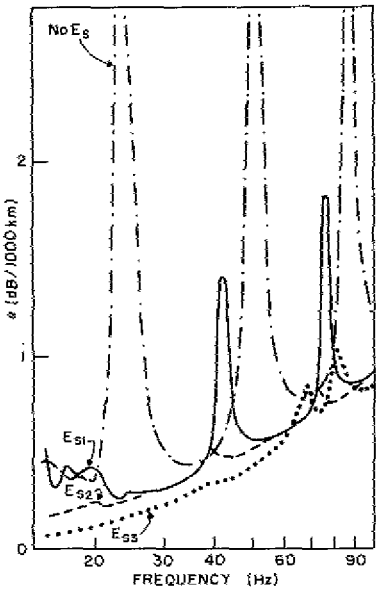

Fig. 12 – Attenuation rate α versus frequency for various conditions of the sporadic E layer

The remaining three curves on Fig. 12 illustrate the effect of introducing varying degrees of sporadic E layers at a 100 km altitude. The solid curve, labeled E_{S1}, represents a condition of moderate sporadic E layers and indicates a condition which can be expected to occur almost

nightly in the auroral region. The resonant peaks are lowered in magnitude relative to the "No E_S" case, as the sporadic E layer reflects more of the ELF energy incident from below; they are displaced downward in frequency as the effective layer separation (in wavelengths) increases due to the added charged-particle density. The lowest resonant peak, which appeared at 23 Hz on the "No E_S" curve, is displaced completely off the lower end of the E_{S1} curve. Enhancement of the sporadic E layer to a maximum density of 10^5 cm^{-3} yields the results indicated by the dashed curve labeled "E_{S2}." The resonant structure has nearly disappeared. Further enhancement of the sporadic E layer to an extreme likely value of 6×10^5 cm^{-3}, represented by the curve labeled "E_{S3}," yields two results. The average attenuation rate is decreased by an amount of about 0.1 dB/1000 km throughout the spectrum, as nearly all the ELF energy is confined below the E layer, and additional resonances begin to appear at the upper end of the spectrum. These new resonances may be attributed to standing waves which are established between the double D-layer ledge at 80 to 90 km and the sporadic E layer at 100 km. Changing the altitude of the sporadic E layer causes the positions of these resonances to shift accordingly.

Figure 13 shows some further aspects of the influence which a sporadic E layer is expected to exert over ELF attenuation rates. The sporadic E layers illustrated in Fig. 12 were all constructed to have about a 5-km thickness, and all appeared as single layers at 100-km altitude. The solid curve in Fig. 13 is similar to the solid curve (denoted E_{S1}) in Fig. 12, except that its thickness has been approximately doubled. This operation causes the resonant attenuation peaks to be depressed by about 0.6 dB/1000 km and lowers their center frequencies by 2 Hz.

It has been found by rocket measurements that sporadic E layers often appear in pairs, with a vertical separation of 6 km to tens of kilometers (28,29). The dotted curve in Fig. 13 represents the effect which a double layer, consisting of sporadic E layers of the E_{S1} type placed at 100 and 112 km, would have on ELF attenuation rates. The resonances are sharpened considerably, and a new resonance peak is beginning to enter from the high-frequency edge of the spectrum. The dashed curve in Fig. 13 shows the effect of raising the upper layer to 124 km. All of the resonant peaks are shifted downward and broadened, and a new resonance appears at 94 Hz.

The polar ionosphere experiences an extensive variation for the period of up to several days following a strong solar flare, due to energetic solar protons which impinge on the lower ionosphere during such a period. At ELF this phenomenon is of great influence because it produces intense ionization throughout the D region above about 60° geomagnetic latitude (nominally the auroral zone and polar cap). Most of the added ionization is produced at altitudes of 40 to 80 km. Reid (30) gives an example of the electron-density profile which might result from a PCA event, and a sketch of such a profile appears in Fig. 14. Also sketched in Fig. 14, for comparison, is the Galejs A profile which has been used in some of the computations above and probably represents normal nighttime conditions below about 100 km. Figure 15 shows the effect on ELF attenuation rates of this PCA electron-density profile, in comparison with the E_{S1} profile in Fig. 12, which probably represents a more realistic approximation of overall normal nighttime

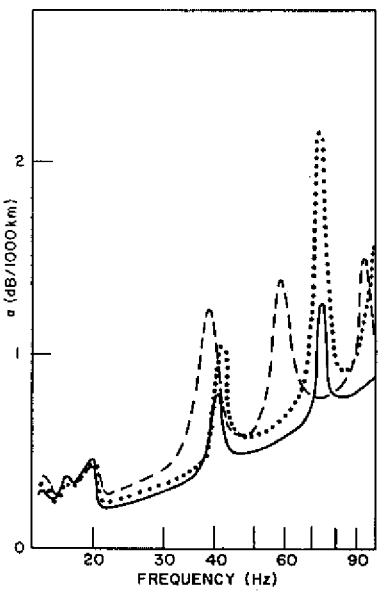

Fig. 13 - Attenuation rate α versus frequency for further variations of the sporadic-E-layer configurations

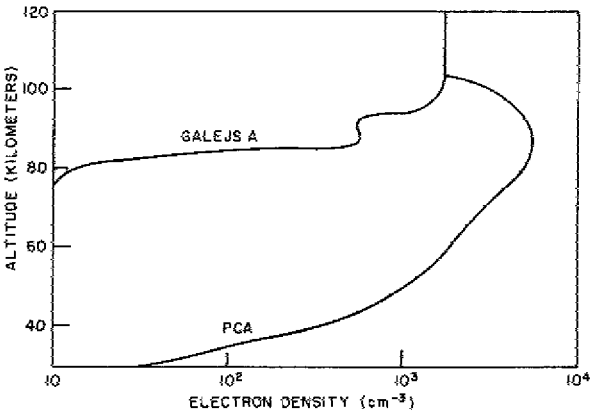

Fig. 14 - Electron-density profiles in D and E layers for propagation calculations by Galejs (25) and for the expected PCA condition

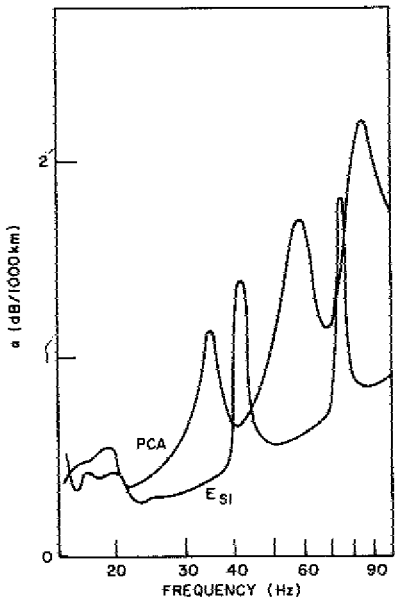

Fig. 15 - Attenuation rate α versus frequency curve for the PCA condition compared with the typical northern-latitude sporadic E condition

conditions than the Galejs A profile. The resonant structure is altered substantially by the PCA event, which introduces an additional resonant peak and broadens all of the peaks relative to the undisturbed resonant structure. There is an obvious degradation in propagation due to the pronounced increase in average attenuation rate across the entire spectrum. This result is in general agreement with those presented by Galejs and Mentzoni (16) for the same PCA event electron-density profile but are substantially different from those presented by Field (18) in which he included the effects of ion-density enhancement in the lower D region in addition to the electron-density increase. It is apparent from Field's results that low-altitude ions associated with a PCA event will cause ELF attenuation rates to be larger in the daytime than values which are computed without considering the effects of these ions. Field did not treat a nighttime PCA case, but observations indicate that the electron density below about 70 km following a PCA event is almost completely removed at sunset (30). Whether the disappearance of this electron-density enhancement arises due to recombination, in which case ELF absorption would be reduced, or due to attachment to neutral molecules, in which case ELF absorption would remain strong, is not reliably known. In the former case, of course, the results presented in Fig. 15 are probably accurate. In the latter case they are certainly underestimates of the actual attenuation rates. For present purposes it can be stated that the resonant structure which appears in the attenuation rate curves for an undisturbed ionosphere will be altered but not removed by a PCA event, and propagation will be degraded due to an overall increase in attenuation across the entire ELF spectrum.

The occurrence of a high-altitude nuclear explosion, at any latitude, can be expected to affect the ionosphere over horizontal regions hundreds to thousands of kilometers in

scale. Once again, the principal effects of such a phenomenon are expected to take place in the lower D region, which is of critical importance for ELF propagation. There have been many attempts to model the electron- and ion-density profiles which appear following a high-altitude nuclear explosion, and the results are so disparate that consideration of any but the simplest of cases is unattractive.

Crain (31) treated the behavior of electron density in the D layer following an assumed uniform ionization impulse of 10^2 to 10^4 cm^{-3} at altitudes from 55 to 115 km. This type of ionization impulse might be expected to result from X rays emitted by a nuclear device exploded above about a 100-km altitude. Figure 16 shows electron-density profiles which would be expected in the nighttime ionosphere at times of 0.1 sec (dotted curve), 1 sec (dashed curve), and 100 sec (solid curve) after such an explosion. These curves take into account reasonable estimates of the usually dominant natural production and loss processes, including electron attachment and electron photodetachment, electron-ion recombination, and ion-ion recombination. In contrast to the PCA example whose electron-density profile was shown in Fig. 14, a high-altitude nuclear explosion yields the greatest enhancement of electron density between 60 and 80 km, with very little enhancement in the 40 to 60 km region in which the solar proton flux, which is responsible for PCA, yielded such a large electron-density enhancement. The peak electron density at shortly after 1 sec following a nuclear explosion would, however, be of the same magnitude and at the same altitude as that due to the PCA example. The effects on ELF attenuation constants might be expected to be somewhat less severe in the nuclear explosion case, however, because the absence of strong ionization below the peak would cause less attenuation.

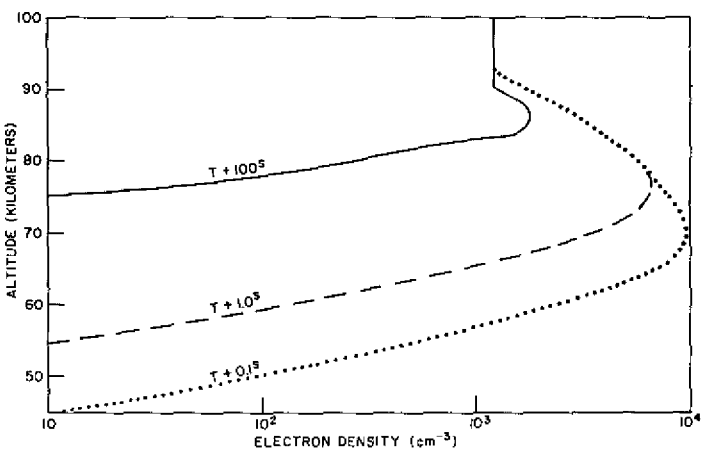

Fig. 16 - Electron-density profiles in D and lower E regions at three times following a high-altitude nuclear explosion

Figure 17 bears out this expectation. The dotted curve, for 0.1 sec after the detonation, indicates that the normally expected resonant structure is greatly attenuated, but the general average level of attenuation between resonant peaks is not increased above that indicated by the curves in Figs. 12 and 13. By 1 sec after the detonation, as shown in the dashed curve, the resonant structure is beginning to emerge, and the general average attenuation level between resonant peaks is lowered even further, especially at high frequencies. This result arises from the fact that ionization below the effective reflection region at about 70 km is disappearing and thus reducing absorption, while the

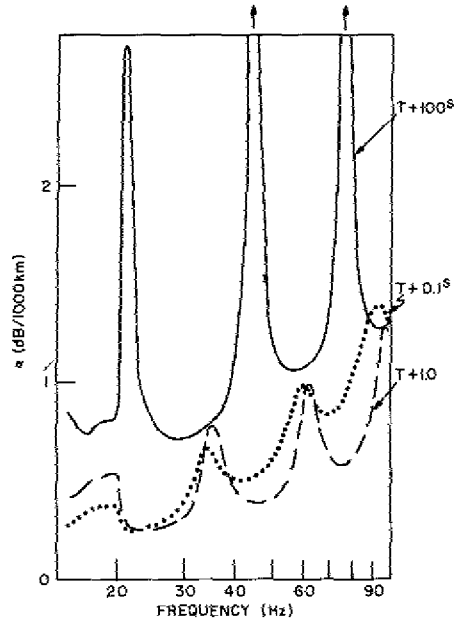

Fig. 17 - Attenuation rate α versus frequency curves for three times following a high-altitude nuclear explosion

relatively high peak electron density continues to prevent energy from leaking into the E and F regions. By 100 sec after the detonation, as shown in the solid curve, the effect of the explosion has nearly disappeared. The exaggerated resonant structure arises, as before, from the oversimplified ionospheric profile. The pronounced increase in attenuation, relative both to the other curves in Fig. 17 and to the curve labeled "No E_S" in Fig. 12, is due to the fact that more energy is leaking into higher ionospheric layers than in earlier stages following the explosion, but a small residue of enhanced ionization persists in the region from 75 to 80 km and hence causes absorption. The final recovery stage would involve a gradual lowering of the solid curve in Fig. 17 to the level displayed by the curve labeled "No E_S" in Fig. 12, as this last-remaining ionization enhancement evaporates. In distinction from the PCA example, the initial few tens of seconds following a high-altitude nuclear explosion should actually cause an improvement in ELF propagation. For some hundreds of seconds thereafter, however, propagation would be expected to be degraded by 0.2 to 0.3 dB/1000 km.

IMPLICATIONS CONCERNING INFORMATION TRANSMISSION

The examples presented in the preceding section suggest that under a variety of conditions the earth-ionosphere waveguide must be considered to be dispersive. The degree to which these idealized examples relate to the actual ionospheric conditions under which a communications system must operate is not known and will remain unknown until an adequate experimental program is undertaken to investigate them. It is likely that the effects of bidirectional propagation, of which examples have been presented in Figs. 2 through 7, will persist to a very significant degree under real conditions. Not only will spatial wave-field irregularities result from the uneven deposition of ELF energy on the earth due to this effect, but transmissions received at even a single station will be degraded due to differential phase dispersion on the two paths over the modulation bandwidth of the transmitted signal. The resonant characteristic of the attenuation rate as a function of frequency, which has been shown in the preceding section to exist under a variety of hypothetical conditions, may correspond less faithfully to reality most of the time for most of the earth. This possibility arises from the likelihood that a great enough variation in ionospheric layer heights and peak electron densities will be encountered along a propagation path many thousands of kilometers long to effectively broaden and attenuate the resonant absorption peaks substantially. The case of polar nighttime propagation, in which northern-latitude sporadic E layers will exist simultaneously over a region thousands of kilometers in scale, suggests that pronounced resonant attenuation effects may actually be experienced on this important path.

Examples to be presented in this section are intended to indicate the extreme of degradation which might occur due to the combination of bidirectional propagation effects, resonant attenuation effects, and additional dispersion due to propagation of ELF signals beneath the ocean surface to a submerged reception terminal. These matters will be

treated in the following subsection. In the second subsection will be presented a brief discussion of the likely extreme of signal degradation which can occur due to spectral contamination of ELF waves penetrating the wavy ocean-surface interface.

Signal Dispersion

Figure 18 contains graphs of attenuation rate and phase velocity for an assumed nighttime ionosphere which might correspond to auroral-zone and polar-cap conditions near a period of relatively high but not uncommon solar activity (such as would occur frequently within a few years of the peak of the 11-year solar cycle). A condition of moderate sporadic E layers, with a peak electron density of 1.4×10^4 cm^{-3}, is assumed to exist at 100-km altitude. An F layer with a peak electron density of 10^6 cm^{-3} is assumed to exist at 290-km altitude. Resonant attenuation-rate peaks occur at 42 and 76 Hz (slight changes in the F-layer height could cause these peaks to appear at other frequencies within a few hertz of these positions). In the frequency bands surrounding these two peaks, an effort has been made to assess the possible effects of dispersion on transmitted information. The basis of this assessment is as follows:

1. An information "pulse," assumed to possess some reasonable waveshape and duration, is Fourier-transformed into the spectral domain.

2. The relative far-field amplitude and phase of spectral components distributed through this spectrum are calculated, based on the attenuation rate and phase velocity indicated on Fig. 18 for each component.

3. An inverse Fourier transform then is applied to the resulting spectrum, converting it back into the temporal domain and hence forming a pulse once more.

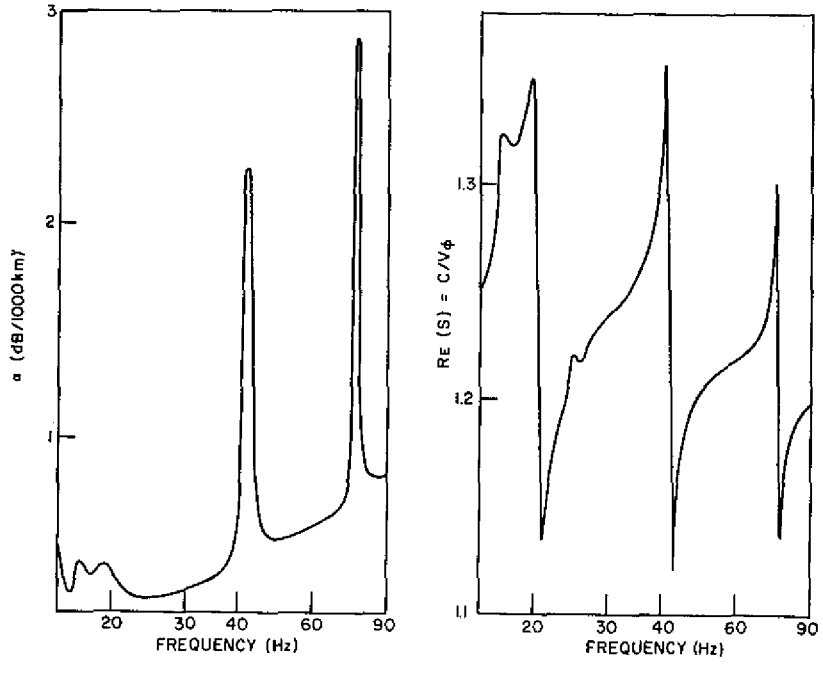

Fig. 18 – Attenuation rate α and phase constant [Re(S)] curves for the likely extreme of the interlayer resonance condition in northern latitudes at night

4. A similar calculation is performed for an identical pulse assumed to traverse the reciprocal path.

5. The two pulses then are summed, with an appropriate time delay between them, to yield an estimate of the total power-versus-time signal which a receiver would detect.

This type of calculation is performed for several ranges between 1000 and 19,000 km from the transmitter. In addition, a dispersion calculation is made for several assumed reception-terminal depths below the ocean surface. Thus the overall effect of dispersion due both to propagation in the earth-ionosphere waveguide and to penetration of several hundred meters of seawater is determined. The method used in this treatment is discussed in greater detail by Uffelman and Davis (32), who also give a number of illuminating examples.

Due to the irregular behavior of the phase-velocity curve in Fig. 18, especially in the vicinity of the resonances at 42 and 76 Hz, determining an appropriate time delay between pulse arrival times at the receiver is by no means straightforward. For so dispersive a medium, a pulse group velocity cannot easily be determined. For the calculations described here, it is assumed that a single pulse is adequately described in the temporal domain by its central lobe plus the first sidelobe. The leading edge of the first temporal sidelobe is assumed to travel at the velocity of light in vacuo. For transmission to distances of at least 10,000 km, it has been found that the pulse maintains enough of its original identity that this leading edge (designated the "precursor") can be discerned. The time delay between the arrival of the precursors on the direct and reciprocal paths then is assumed to be the difference in path length divided by the speed of light in vacuo. For some cases, in which the precursor cannot be identified beyond about 10,000 km, its further dispersion is assumed to obey the same dependence on range as it does on the average over the interval from 5000 to 10,000 km.

Figure 19 contains spectral- and temporal-domain plots of a minimum-frequency-shift-keyed (MSK) pulse of about 0.5-sec duration (principal temporal lobe width) whose spectrum is centered on 43 Hz. These examples do not include the effect of seawater dispersion and represent only the degradation which would result from transmission in the earth-ionosphere waveguide. They also show only the direct-path signal, and so interference effects from bidirectional propagation are also excluded. The left-hand column contains spectral representations of the waveform at ranges of 0, 5000, 10,000, and 15,000 km from the transmitter. The center column contains temporal representations of the same waveforms, with a linear amplitude scale. The slanted line which appears between the bottom-three graphs in this column indicates the estimated precursor positions from which pulse time delay was calculated. The right-hand column contains logarithmic representations of these same temporal waveforms, shown here with a dynamic range of 40 dB. These graphs are calibrated relative to an assumed transmitter dipole moment of 3×10^7 A·m. It is evident that significant dispersion occurs even on the shortest (5000-km) path. On the basis that a signal-to-noise ratio (SNR) of 10 dB is required for minimally acceptable information transmission, it is apparent that information rates must be reduced by a factor of at least 2, based on dispersion on the direct path alone. For a more realistic requirement of a 20-dB SNR, the situation is degraded even further.

Figure 20 is a quasi-three-dimensional-surface plot, on the same 40-dB logarithmic scale, showing how the form of the pulse is distorted in transmission over ranges of 1000 to 19,000 km, including the effects of seawater dispersion to an assumed depth of 400 m. The axis which appears to jut out of the page is logarithmic amplitude. This plot shows the top 40 dB occupied by the pulse at any range, and so the overall attenuation-versus-range effect is removed. Only amplitude relative to other temporal positions within the same trace is accurately represented. The appearance and growth of temporal sidelobes

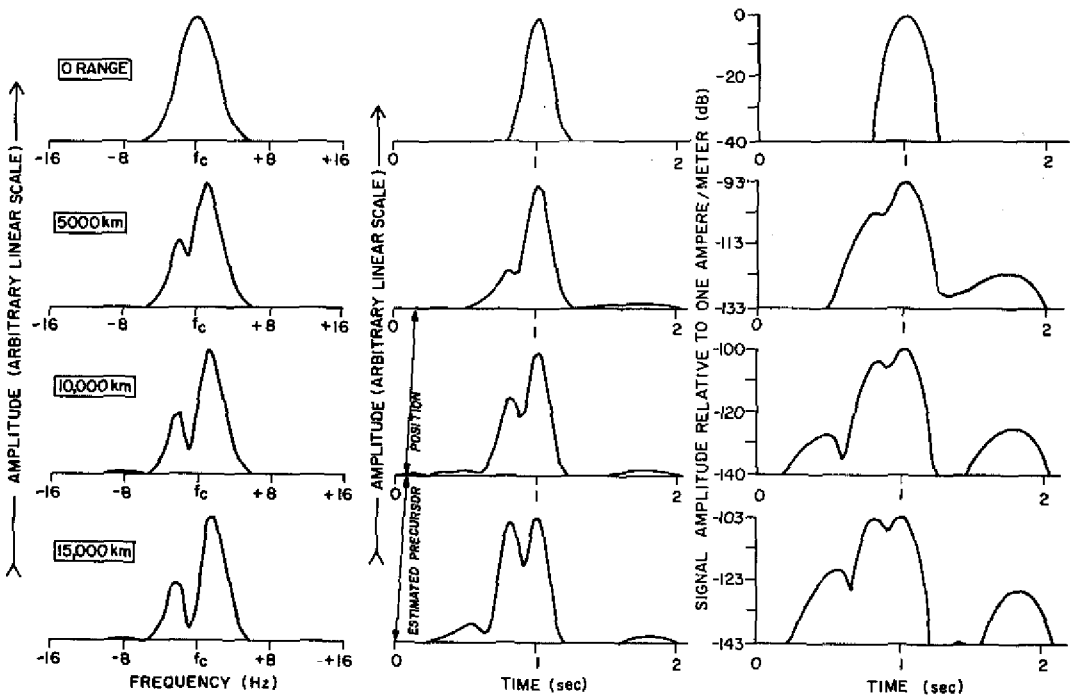

Fig. 19 – Spectral- and temporal-domain plots of a 0.5-second MSK pulse as it appears at the transmitter (labeled 0 range) and at 5000, 10,000, and 15,000 km from the transmitter. The estimated position of the precursor is labeled in the center column. The transmitted spectrum is centered on 43 Hz.

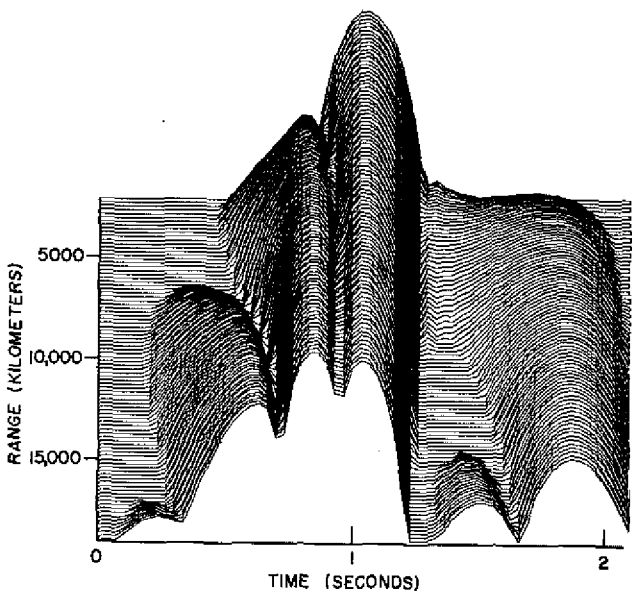

Fig. 20 – Quasi-three-dimensional logarithmic (40-dB) plot showing pulse distortion with distance on a short path. The transmitted spectrum is centered on 43 Hz. The receiving terminal is 400 m below the surface.

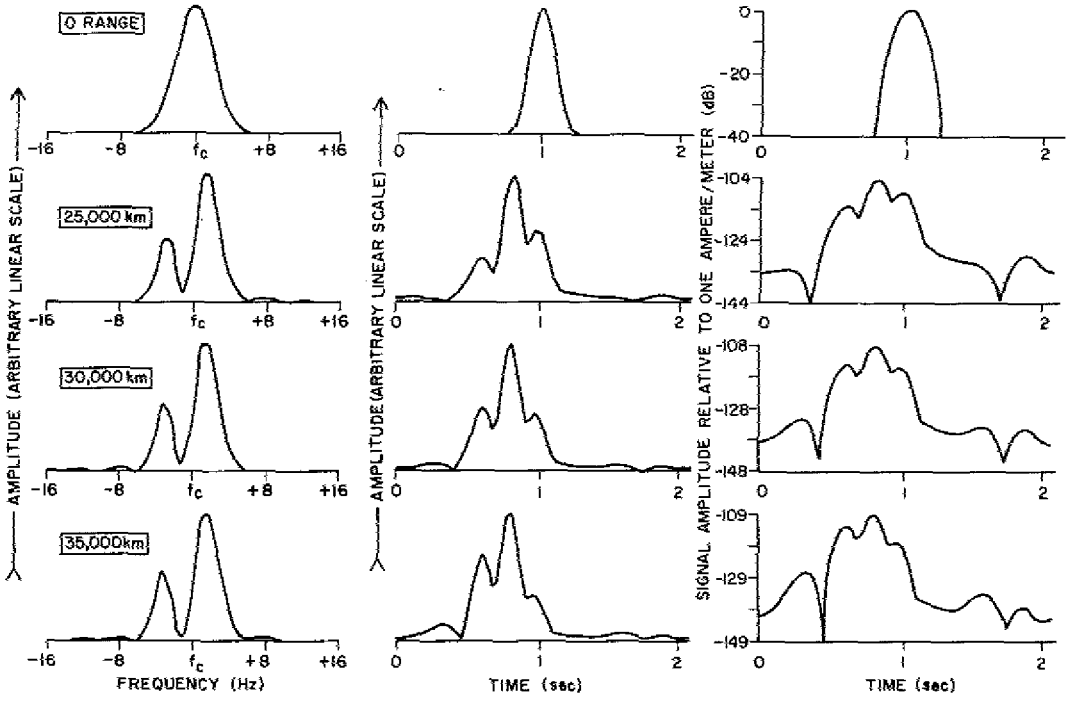

Fig. 21 - Spectral- and temporal-domain plots of a 0.5-second MSK pulse as it appears at the transmitter and at 25,000, 30,000, and 35,000 km from the transmitter. The transmitted spectrum is centered on 43 Hz.

with increasing range is evident; the effect of seawater dispersion is readily seen to be negligible by comparison with Fig. 19.

Figure 21 contains spectral- and temporal-domain representations of pulses transmitted at the same center frequency and duration as Fig. 20, for the reciprocal path lengths of 25,000, 30,000, and 35,000 km. To include possible effects of nonreciprocal propagation and to cause these examples to represent a probable worst case, the attenuation rates at all frequencies were assumed to be reduced by 30% in these long-path calculations relative to the values in Fig. 18. The resultant waveforms, which appear on a 40-dB logarithmic scale in the right-hand column, are degraded considerably relative to those in Fig. 19. Figure 22 is a surface plot for the long-path signal, showing the development of the extremely prominent temporal sidelobes which appear.

Figure 23 contains logarithmic temporal plots of the summed contributions from both paths, at distances of 0, 5000, 10,000, and 15,000 km and at depths below the ocean surface of 0, 200, and 400 m. The effects of two-path interference are evident. Signal degradation at the -10-dB level is not much worse than in Fig. 19, but at the -20-dB level it is significantly worse at most distances.

Figures 24 through 28 contain results for a similar pulse format at an assumed center frequency of 77 Hz. The summed waveforms in Fig. 28 are qualitatively similar to those for 43 Hz in Fig. 23.

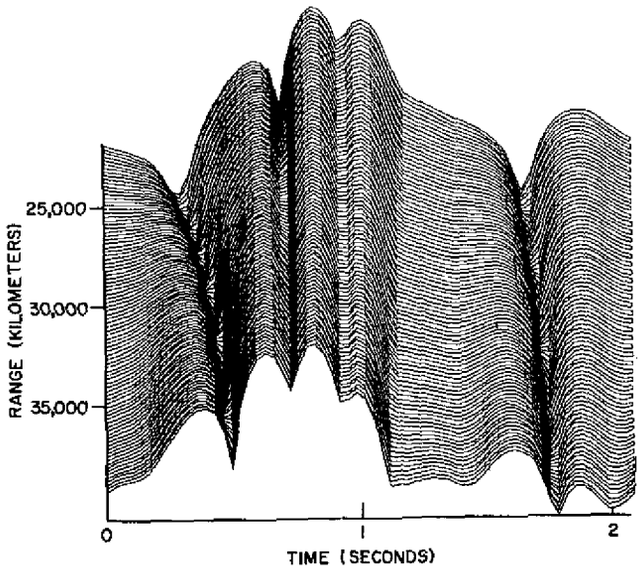

Fig. 22 – Quasi-three-dimensional logarithmic (40-dB) plot showing pulse distortion with distance on a long path. The transmitted spectrum is centered on 43 Hz. The receiving terminal is 400 m below the surface.

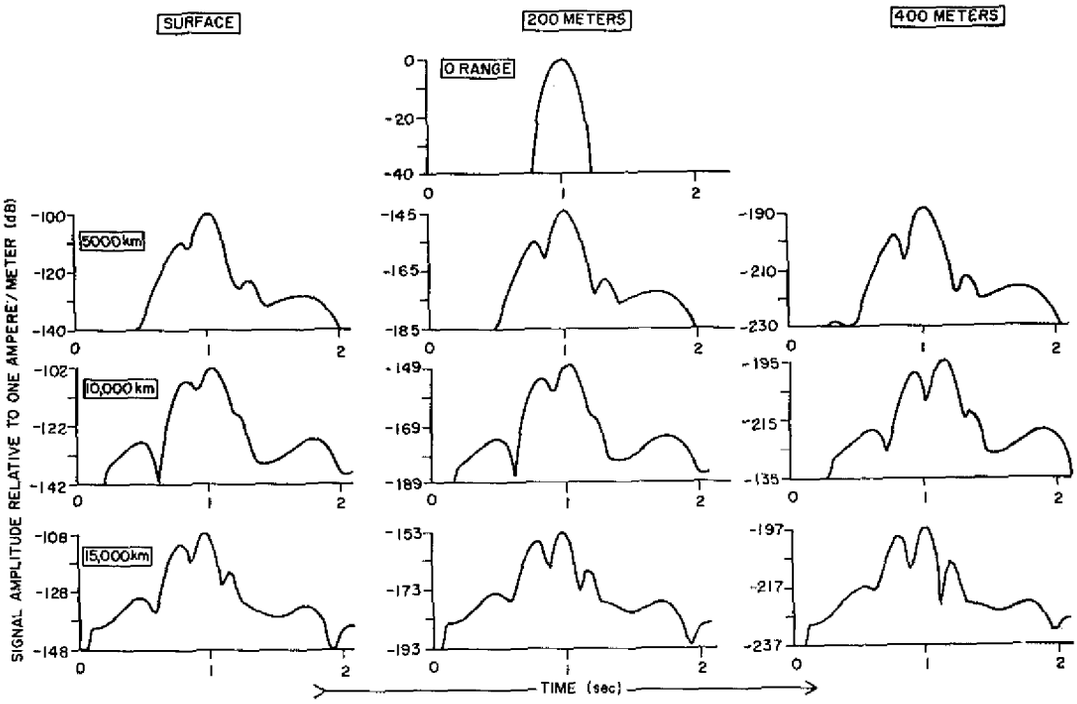

Fig. 23 – Total received pulse at the surface and at depths of 200 and 400 m for a receiver located 5000, 10,000, and 15,000 km from a transmitter radiating a 0.5-second MSK pulse centered on 43 Hz.

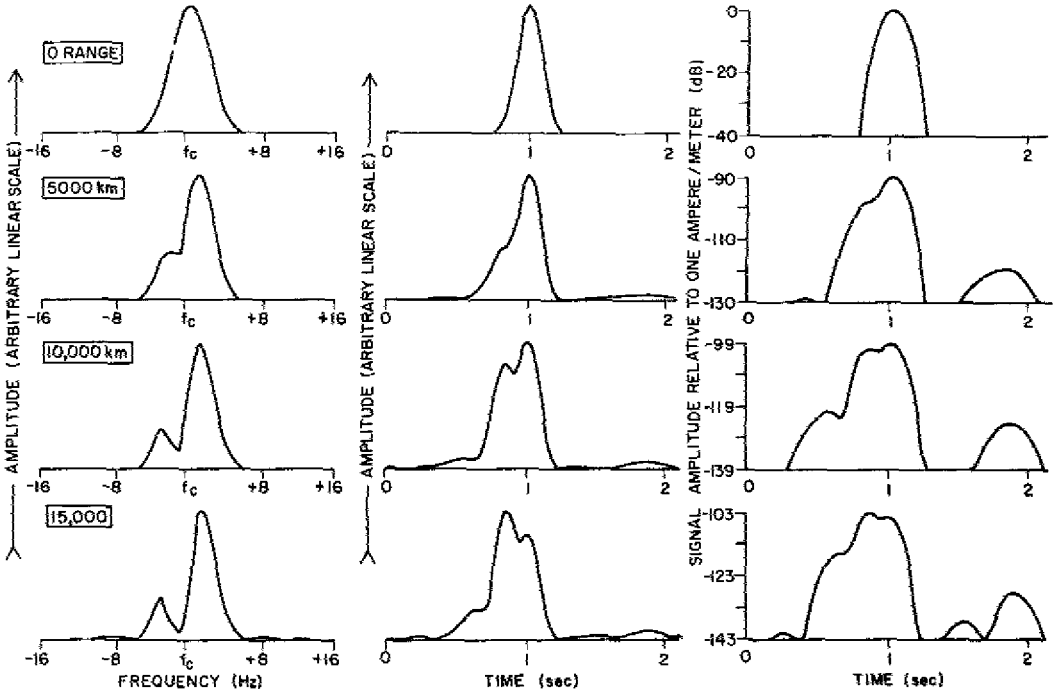

Fig. 24 - Spectral- and temporal-domain plots of a 0.5-second MSK pulse as it appears at the transmitter and at 5000, 10,000, and 15,000 km from the transmitter. The transmitted spectrum is centered on 77 Hz.

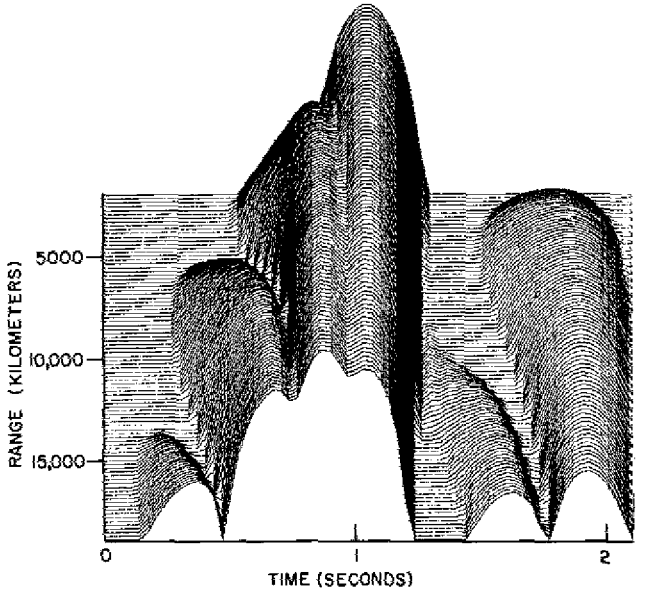

Fig. 25 - Quasi-three-dimensional logarithmic (40-dB) plot showing pulse distortion with distance on a short path. The transmitted spectrum is centered on 77 Hz. The receiving terminal is 400 m below the surface.

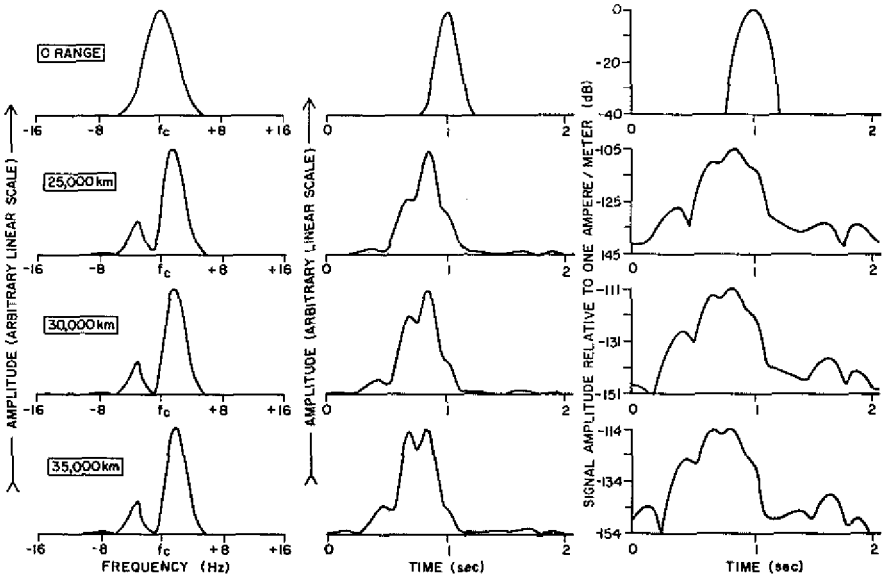

Fig. 26 - Spectral- and temporal-domain plots of a 0.5-second MSK pulse as it appears at the transmitter and at 25,000, 30,000, and 35,000 km from the transmitter. The transmitted spectrum is centered on 77 Hz.

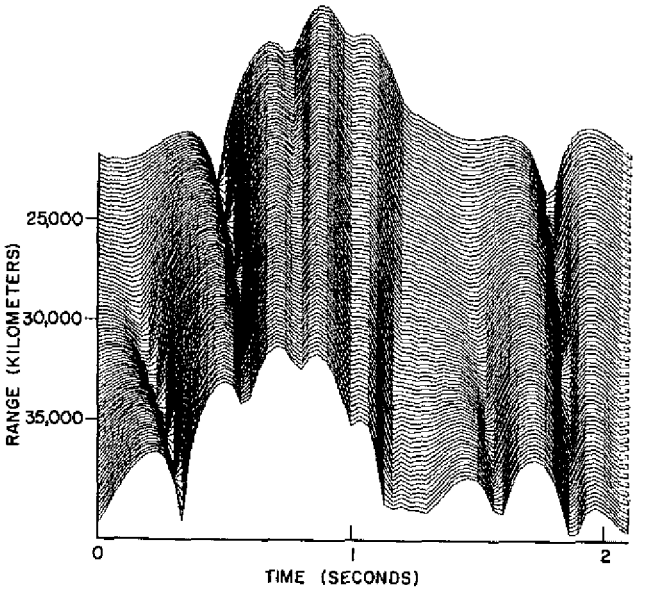

Fig. 27 - Quasi-three-dimensional logarithmic (40-dB) plot showing pulse distortion with distance on a long path. The transmitted spectrum is centered on 77 Hz. The receiving terminal is 400 m below the surface.

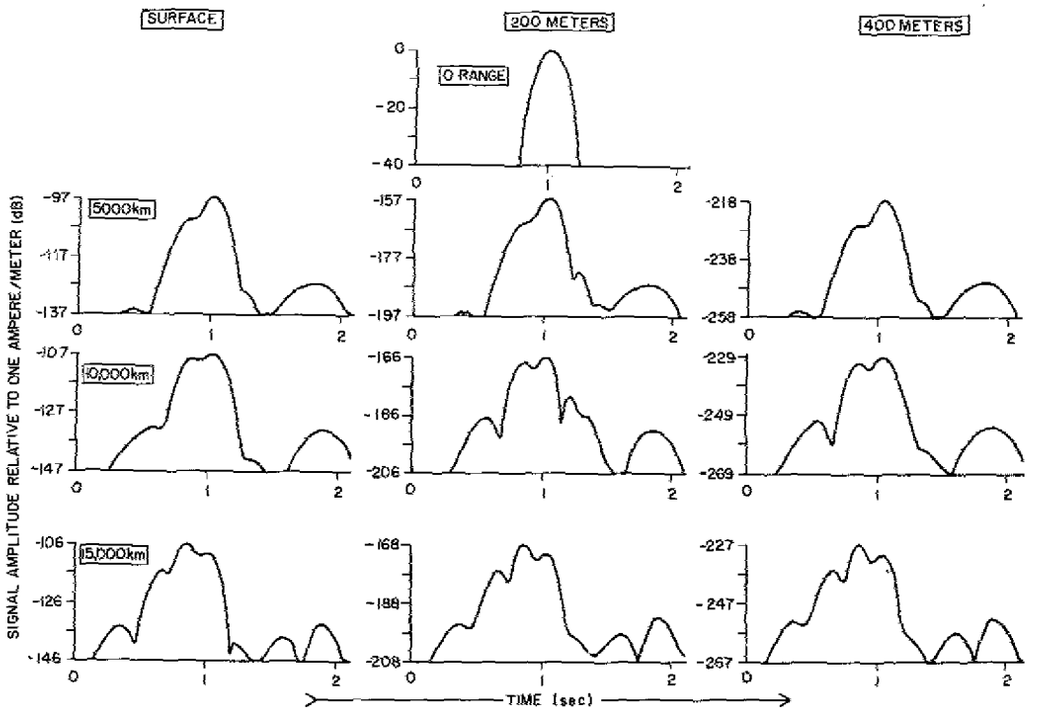

Fig. 28 – Total received pulse at the surface and at depths of 200 and 400 m for a receiver located 5000, 10,000, and 15,000 km from a transmitter radiating a 0.5-second MSK pulse centered on 77 Hz

It can be concluded that the dispersion which results from the resonant character of the ionospheres treated in this report might, indeed, lead to degradation in communication information rates by a factor exceeding 2 for pulse lengths of 1/2 second or shorter. A good deal of caution should be exercised in interpreting the word "might" as meaning "will," however. The ionospheric models are hypothetical ones, and the F-layer electron-density profiles are somewhat unrealistic. These results should accordingly be interpreted as upper limits on the degree of degradation which can arise from propagation-associated phenomena. It is of some interest that dispersion due to the variation of seawater attenuation with frequency is negligible in comparison to that introduced by the ionosphere. Indeed, the former type of dispersion can be considered to be a second-order effect by comparison to the latter for the cases treated in this report.

Water-Wave Spectral Contamination

Transmission of ELF energy across the ocean surface can be expected to result in spectral degradation of the signal due to fluctuation components introduced by the wave motions on that interface. Wetzel (33) describes approximate methods by which the levels (amplitudes) and spectral characteristics of these fluctuations can be estimated to affect ELF waves penetrating the ocean surface and propagating through it to a receiver terminal at arbitrary depth. Under certain assumptions, notably the basic assumption that a wind-driven water wave can be described as a sinusoid of some particular amplitude and wavelength, Wetzel uses empirical estimates of the relationship between these parameters and wind speed to derive expressions for the fluctuation level and spectrum which might be expected for typical ocean-wave spectra. The treatment Wetzel employs

is restricted in applicability to certain water wavelengths; for frequencies in the range from 45 to 75 Hz, this restriction limits its use to conditions involving wind speeds of less than about 100 knots and hence represents no significant limitation.

The integral for the fluctuation level relative to an undisturbed ELF signal can be evaluated only for rather simple water-wave spectra. One case for which the integral is tractable is a monotonic spectrum corresponding to the simple circumstance of "swell" alone. Table 3 contains the results of such a calculation for wind speeds of 10 to 50 m/sec (20 to 100 knots) as they affect ELF waves of 45 and 75 Hz propagating to depths of 50 to 400 meters below the ocean surface. Heavy lines indicate a fluctuation level 10 to 20 dB below the undisturbed signal level. If fluctuation levels of this magnitude are accepted as leading to significant spectral degradation of the signal, then wind speeds of 20 to 35 m/sec (40 to 70 knots) must be considered as serious potential contaminants in a communication network.

Table 3
Fluctuation Levels for Swell Waves Generated by Winds of Various Speeds

Wind Speed (m/sec)	Fluctuation Level at Four Depths Relative to Undisturbed Signal (dB)							
	45 Hz				75 Hz			
	50 m	100 m	200 m	400 m	50 m	100 m	200 m	400 m
10	-71	-102	-164	-289	-63	-91	-147	-259
15	-35	-43	-60	-94	-29	-36	-49	-76
20	-22	-25	-30	-40	-19	-21	-25	-33
25	-16	-17	-19	-23	-14	-14	-16	-19
30	-12	-13	-14	-16	-10	-10	-11	-13
35	-9	-10	-10	-11	-7	-7	-8	-9
40	-7	-7	-8	-8	-5	-5	-5	-6
45	-5	-5	-5	-6	-3	-3	-3	-3
50	-3	-3	-3	-4	Beyond Applicable Limits			

The degree to which such contaminants might limit information transmission can be estimated by considering the form which this spectral contamination might take. Wetzel's treatment permits calculating the power spectrum from a more realistic water-wave spectrum than the monotonic one discussed in the preceding paragraph. The Pierson-Moskowitz water-wave energy spectrum is characterized by a frequency dependence of the form

$$\frac{1}{\omega^5} e^{-0.74(g/W\omega)^4} ,$$

where ω is frequency, g is the acceleration of gravity, and W is the wind speed (mks units). The results of the calculation, for wind speeds from 20 to 50 m/sec and receiver

depths of 50, 200, and 400 m, are shown in Figs. 29 through 31. Examples are shown only for a radio frequency of 45 Hz. The general trend with increasing depth is a narrowing of the spectrum from its high-frequency end with little or no displacement in spectral peak positions. The principal value of Figs. 29 through 31 is in estimating likely limits on signal integration time which water-wave spectral contamination might impose. For example, a wind speed of 30 m/sec will impose on a 45-Hz electromagnetic wave received at a 50-m depth (Fig. 29) a fluctuation component with a spectral peak at 0.044 Hz. Thus for integration times of about 23 sec and shorter, the fluctuation component will

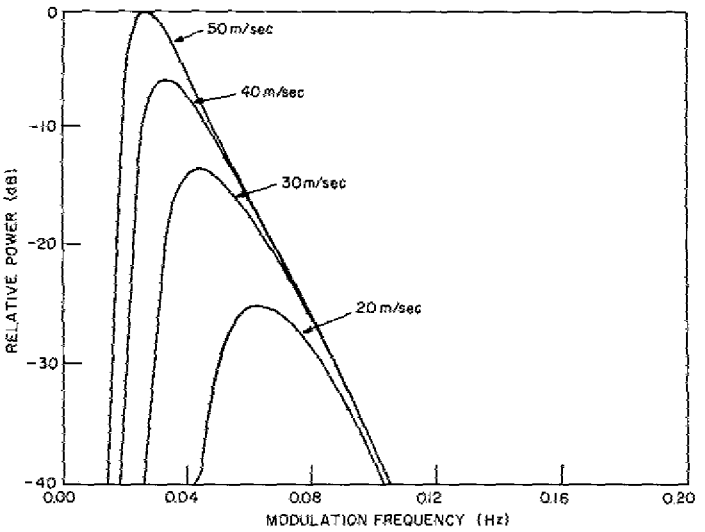

Fig. 29 - Fluctuation spectrum due to water waves driven by winds of indicated speeds as observed at a 50-m depth

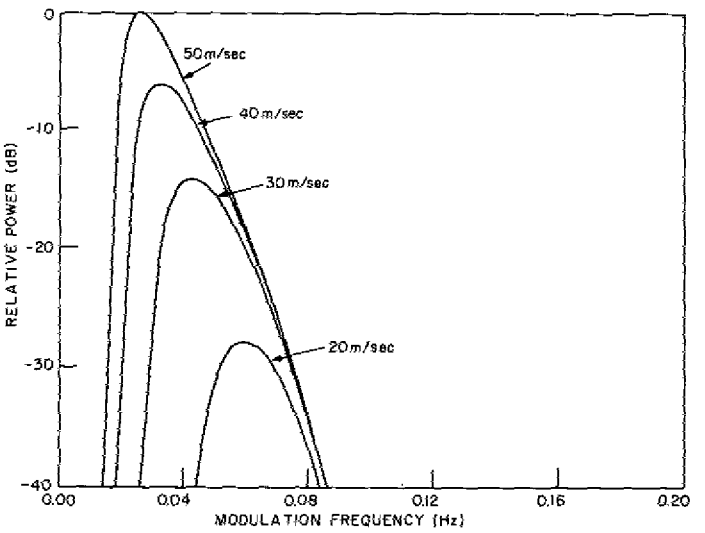

Fig. 30 - Fluctuation spectrum due to water waves driven by winds of indicated speeds as observed at a 200-m depth

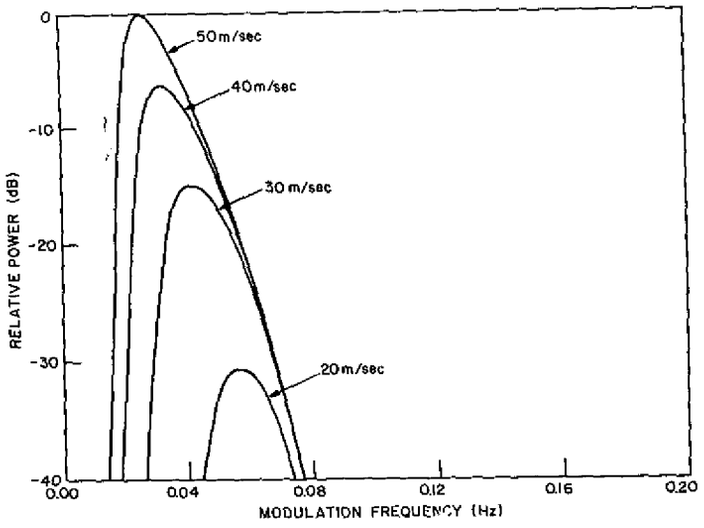

Fig. 31 - Fluctuation spectrum due to water waves driven by winds of indicated speeds as observed at a 400-m depth

begin to contribute to the total received signal and cannot be filtered out. For longer integration times, it can be effectively removed if the modulation bandwidth is narrower than about 0.030 Hz.

It can be concluded that spectral contamination of ELF waves crossing the ocean surface may be encountered at wind speeds of 20 m/sec (40 knots) and greater. When this spectral contamination is a problem, it can cause the available modulation bandwidth to be narrowed to a few hundredths of a hertz.

RECOMMENDATIONS FOR EXPERIMENTAL STUDIES

Every aspect of ELF propagation discussed in this report lacks adequate experimental verification. Furthermore, the subjects treated in this report indicate that a measurement program whose object is to provide this necessary verification must be planned with care. The various effects described above are all likely to occur in varying degrees simultaneously; hence it will be difficult to isolate them for systematic study. First, for example, isolation of geomagnetic anisotropy of propagation from the possibly similar effect of diurnal asymmetry of the earth-ionosphere waveguide requires that measurements be taken under conditions in which both easterly and westerly paths are equally sunlit or dark. Second, the possible effects of differing F-layer height, in imposing resonancelike behavior on the attenuation-rate-versus-frequency curve, requires that any nighttime measurements be made under conditions in which the upper ionosphere is identical on both paths. Such conditions seldom coincide precisely with the desired symmetry of path darkness because the ionosphere's physical chemistry causes its diurnal evolution to lag the solar day. Third, the possible influence of bidirectional propagation requires these measurements to be made such that the spatial wave-field distribution due to two-path interference is well known in both the easterly and westerly directions. If there is, indeed, significant propagation anisotropy, the spatial wave-field distribution will certainly vary differently in the two directions. These considerations alone indicate that an effective measurement program must involve several receiving sites in simultaneous operation and must be approached systematically.

The following list of suggested experiments is intended only as an indication of an efficient order of priorities in conducting such an experimental program.

1. Assessment of geomagnetic-anisotropy and bidirectional-propagation effects in the sunlit hemisphere. Assuming attenuation rates to be greater for westerly than for easterly propagation, one station should be located at about 5000 km and two or more stations at about 10,000 km west of the transmitting site. One station should be located about 5000 km east of the transmitting site. Measurements should be restricted to a period beginning about 2 hours before noon at the transmitter and ending about 4 hours after noon at that site. An effort should be made to determine whether there exists a difference in apparent attenuation rates from the transmitter to each of the close-in sites. The two or more sites located about 10,000 km west of the transmitter should be separated by about 2000 km and should attempt to discern wave-field interference patterns due to bidirectional propagation. Care must be taken at these sites to insure that evening twilight does not introduce uncertainties into the measurements; hence operations should probably be restricted to the period before noon at the transmitter site. Because ELF waves probably do not penetrate the E layer in the sunlit hemisphere, there should be no interlayer resonant effect.

2. Assessment of geomagnetic-anisotropy, bidirectional-propagation, and interlayer-resonance effects in the darkened hemisphere. Due to the increased depth of penetration of ELF waves into the E and F layers at night, both geomagnetic-anisotropy and interlayer-resonance effects will be more pronounced than in daytime. The same receiving sites may be used, but many more measurement periods may be necessary. A similar type of operation to that described in assessment 1 may be used, but the reference time should be midnight at the transmitter rather than noon. To determine the effects of interlayer resonances, a frequency-sweeping or stepping mode will be necessary. The transmitted frequency should be deviated 5 to 10 Hz on both sides of the nominal center frequency, with dwell times equal to a minimum acceptable integration time for the receiving sites. The close-in sites will probably suffice for this frequency-deviating phase of the measurements, and so dwell times may be tailored to their requirements.

3. Assessment of diurnal anisotropy in propagation. Measurements of the apparent attenuation rates for easterly and westerly propagation should be made during both morning and evening twilight at the transmitter site. The close-in sites should provide estimates of the propagation anisotropy. Further measurements of bidirectional propagation may also be made at receiving sites in the range 10,000 to 18,000 km, located preferably both to the east and west of the transmitter. It is only with the twilight discontinuity located directly over the transmitter that paths may be set up which are all dark and all sunlit so that this phenomena may be isolated from twilight-zone discontinuities in the earth-ionosphere waveguide.

4. Assessment of the effects of waveguide discontinuities on propagation. Passage of the twilight region over the receiving sites will permit spatial wave-field irregularities which arise from the associated waveguide discontinuities to be discerned. Integration times should be kept as short as possible; hence only the close-in receiver sites may be useful. Measurements should be made from about 4 hours before until 4 hours after both morning and evening twilight (the ionosphere changes at a different rate in each period).

5. Assessment of auroral and PCA effects on propagation. Measurement of these effects must take place during arctic winter, so that the dark-path conditions under which effects of PCA and auroral events are most pronounced will be tested. In order that these measurements, which will involve precisely the propagation paths of importance for an operational communications system, will fully reflect the ionospheric conditions which will be encountered in the polar region, stations should be located in several areas.

For a transmitter located in Wisconsin, a station in eastern Scandinavia will be about 5000 km from the transmitter and on the Atlantic fringe of the auroral region. A station in the Aleutians will be at a similar range on the Pacific fringe. A station on Okinawa will be about 9000 km from the transmitter and on the longest possible line through the zone of maximum auroral activity. A station in South Korea will be 10,000 km from the transmitter and on a line which passes through the fringe of the polar cap. A station in Indochina, India, or Pakistan will be 13,000 km from the transmitter and on a line nearly through the geomagnetic north pole. These stations should be established for several months and operated routinely during the two to five days following strong solar flares. It is expected that the influence of interlayer-attenuation-rate resonances, which may be quite pronounced during normal auroral and polar nighttimes (to be discussed under assessment 6), will be substantially diminished during these disturbed periods. This thesis may be tested by using the frequency-deviating method discussed in assessment 4.

6. Assessment of auroral-zone sporadic E effects on propagation. The most extreme examples of interlayer resonance effects should be expected to occur during arctic winter on the paths listed in assessment 5. Thus these stations should be operated frequently during times of solar quiescence, and the transmitter should be run in the frequency-deviating mode.

ACKNOWLEDGMENT

The authors are grateful for the benefit of many helpful discussions with Dr. Janis Galejs of the Advanced Studies Group, Communications Sciences Division, and for generosity by Mr. F. M. Gager and Mr. P. E. V. Shannon of the Radar Techniques Branch, Radar Division, in making computational facilities available for this research.

REFERENCES

1. Chapman, F.W., and Macario, R.C.V., "Propagation of Audio-Frequency Radio Waves to Great Distances," Nature 177, 930-933 (1956)

2. Chapman, F.W., Jones, D.L., Todd, J.D.W., and Challinor, R.A., "Observations on the Propagation Constant of the Earth-Ionosphere Waveguide in the Frequency Band 8 c/s to 16 kc/s," Radioscience 1, 1273-1282 (1966)

3. Hughes, H.G., "On the Directional Dependency of 'Slow Tail' Extremely Low-Frequency Atmospheric Waveforms," J. Atm. and Terres. Physics 29, 545-552 (1967)

4. Smith, E.J., "The Propagation of Low-Audio Frequency Electromagnetic Waves," Ph.D. Thesis, UCLA, 1960

5. Hughes, H.G., "Nonreciprocal Attenuation Rates at ELF from 'Slow Tail' Measurements," JGR 72, 5383-5388 (1967)

6. Hughes, H.G., and Thiesen, J.F., "Diurnal Variations in the Apparent Attenuations of ELF Atmospherics over Two Different Propagation Paths," J. Geophys. Res. 75, 2795-2801 (1970)

7. Hughes, H.G., and Thiesen, J.F., "Propagation of the 50-Hz Spectral Component of ELF Atmospherics Across the Sunrise Terminator," NELC Report 1643, Aug. 19, 1969

8. Jones, D.L., "Propagation of ELF Pulses in the Earth-Ionosphere Cavity and Application to 'Slow Tail' Atmospherics," Radioscience 5, 1153-1162 (1970)

9. Taylor, W.L., and Sao, K., "ELF Attenuation Rates and Phase Velocities Observed From Slow Tail Components of Atmospherics," Radioscience 5, 1453-1460 (1970)

10. Chapman, F.W., and Jones, D.L., "Observations of Earth-Ionosphere Cavity Resonances and Their Interpretation in Terms of a Two-Layer Ionosphere Model," J. Res. NBS 68D, 1177-1185 (1964)

11. Dunn, G.R., Kuhnle, P.F., and Smith, R.D., "Experimental Research Investigations of Extremely Low Frequency Propagation," Space-General Corporation Technical Report SGC No. 212R-8, Feb. 28, 1964

12. Kuhnle, P.F., and Smith, R.D., "Experimental Research Investigation of Extremely Low Frequency Propagation," Technical Documentary Report No. RADC-TDR-64-360, RADC, December 1964

13. Galejs, J., "ELF and VLF Waves Below an Inhomogeneous Anisotropic Ionosphere," J. Res. NBS 68D, 693-707 (1964)

14. Galejs, J., "On the Terrestrial Propagation of ELF and VLF Waves in the Presence of a Radial Magnetic Field," J. Res. NBS 69D, 705-720 (1965)

15. Galejs, J., "Propagation of ELF and VLF Waves Below an Anisotropic Ionosphere With a Dipping Static Magnetic Field," J. Geophys. Res. 73, 339-352 (1968)

16. Galejs, J., and Mentzoni, M., "Propagation of ELF and VLF Waves Below Models of Naturally Perturbed Ionospheres," J. Geophys. Res. 73, 4439-4443 (1968)

17. Galejs, J., "ELF and VLF Propagation for Models of a Perturbed Ionosphere," Radioscience 5, 1041-1044 (1970)

18. Field, E.C., "Propagation of ELF Waves Under Normal and Naturally Disturbed Conditions," J. Geophys. Res. 74, 3639-3650 (1969)

19. Yamashita, M., "Propagation of E.L.F. Radio Waves to Great Distances Below the Anisotropic Ionosphere," J. Atm. and Terres. Physics 29, 937-948 (1967)

20. Yamashita, M., "The Propagation Characteristics of ELF Radio Waves to Great Distances Below the Horizontally Stratified Ionosphere," J. Atm. and Terres. Physics 30, 1943-1953 (1968)

21. Jones, D.L., "Schumann Resonances and E.L.F. Propagation for Inhomogeneous, Isotropic Ionosphere Profiles," J. Atm. and Terres. Physics 29, 1037-1044 (1967)

22. Cole, R.K., Jr., and Pierce, E.T., "Electrification in the Earth's Atmosphere for Altitudes Between 0 and 100 Kilometers," J. Geophys. Res. 70, 2735-2749 (1965)

23. Deeks, D.G., "D-Region Electron Distributions in Middle Latitudes Deduced From the Reflexion of Long Radio Waves," Proc. Roy. Soc. 291, 413-437 (1966)

24. Kelly, F.J., NRL Report in preparation

25. Galejs, J., "F Layer Reflections and Ion Effects in the Propagation of Terrestrial ELF Waves," J. Geophys. Res. 75, 2529-2539 (1970)

26. Galejs, J., Terrestrial Propagation of Long Electromagnetic Waves, Chapter 7, monograph in preparation

27. Smith, E.K., Jr., "The Occurrence of Sporadic E," in Ionospheric Sporadic E, E.K. Smith, Jr. and S. Matsushita, Pergamon Press, N.Y., 1962, pp. 3-12

28. Aubry, M., Blanc, M., Clauvel, R., Taieb, C., Bowen, P.J., Norman, K., Willmore, A.P., Sayers, J., and Wager, J.H., "Some Rocket Results on Sporadic E," Radioscience 1, 170-177 (1966)

29. Smith, L.G., "Rocket Observations of Sporadic E and Related Features of the E Region," Radioscience 1, 178-186 (1966)

30. Reid, G.C., "Physics of the D Region at High Latitudes," in J. Frihagen (ed.), Electron Density Profiles in Ionosphere and Exosphere, North-Holland, Amsterdam, Interscience, N.Y., 1966, pp. 17-26

31. Crain, C.M., "Electron Ionization and Loss Processes and Rates," in J. S. Belrose, I. A. Bourne, and L. W. Hewitt (compilers), Ground-Based Radio Wave Propagation Studies of the Lower Ionosphere, Defence Research Board, Dept. of National Defence, Ottawa, Ontario 1967

32. Uffelman, D.R., and Davis, J.R., "Computer Simulation of ELF Pulse Distortion due to Dissipation and Dispersion in the Earth-Ionosphere Waveguide," NRL Report in preparation

33. Wetzel, L., "Electromagnetic Field Fluctuations in Transmission through the Surface of the Sea," Proceedings of the NATO AGARD Symposium on Electromagnetics of the Sea, Paris, France, June 1970